Universität Bonn

Physikalisches Institut

Modeling and measuring the $t\bar{t}\gamma$ process with the ATLAS detector at 8 TeV

Sebastian Heer

The Monte Carlo generators for the $t\bar{t}\gamma$ process are available in leading order and next-to-leading order. Using a next-to-leading order generator features a better precision. Due to a large amount of possible diagrams for the $t\bar{t}\gamma$ process however, the next-to-leading order generators are not able to accurately describe photons radiated from the decay products of the top quark. Leading order generators on the other hand are able to have photons in the final state. This includes interference effects of initial and final states, which cannot be described by next-to-leading order generators. With the addition of a QED generator, to simulate the final state photons, the modeling of leading order and next-to-leading-order generators are studied.
The cross section of $t\bar{t}\gamma$ production in collisions of protons is predicted by the Standard Model and has to be measured by experiment. The measurement presented in this thesis is done using $t\bar{t}\gamma$ events in the dilepton channel. Dileptonic events were not used for the $t\bar{t}\gamma$ process in general yet, because of the small branching fraction. The analysis uses events from the eμ-channel only, because of the very high signal-to-background ratio, which is not blurred by background processes involving the Z boson. A cut-and-count method is used for the measurement. To get the optimal set of requirements for the measurement, the event selection was optimized by minimizing the relative uncertainty on the expected cross section.

Physikalisches Institut der
Universität Bonn
Nussallee 12
D-53115 Bonn

BONN-IB-2016-03
Dezember 2015

Universität Bonn

Physikalisches Institut

Modeling and measuring the $t\bar{t}\gamma$ process with the ATLAS detector at 8 TeV

Sebastian Heer

Dieser Forschungsbericht wurde als Masterarbeit von der Mathematisch-Naturwissenschaftlichen Fakultät der Universität Bonn angenommen.

Angenommen am:	22.12.2015
1. Gutachter:	Dr. Markus Cristinziani
2. Gutachterin:	Prof. Dr. Norbert Wermes

Acknowledgements

First, I would like to thank Dr. Markus Cristinziani for introducing me into the group, supervising my thesis and always offering help when needed, regardless of helping me for my thesis or offering personal requests.
I would like to thank Prof. Dr. Norbert Wermes for being the second referee of my thesis and for welcoming me into the group. Also he provided the necessary facilities to work in a pleasant environment, for which I am very grateful.
Furthermore I would like to thank Dr. Liza Mijović for supervising my thesis and for the long and interesting discussions that helped me to progress with this thesis.
I would like to thank the members of Dr. Markus Cristinziani's research group and members of my office, Nello Bruscino and Dr. Kaven Yau Wong who kindly welcomed me into the group and were always available for help. Without their support, I would not have been able to polish my programming skills, which made many of the calculations done for this thesis possible. Also I would like to thank the members of the group who joined after me, Mazuza Ghneimat, Evan Machefer and Andrea Sciandra, which I enjoyed talking to during meetings and lunch breaks and who also were always offering their help. I would also like to add Dr. Vadim Kostyukhin, who usually stays at CERN, but visits Bonn once per month as member of the group and was always willing to explain the most advanced problems in physics. Additionally I would like to thank my group for proof-reading this thesis and providing me with additional figures.
Finally I would like to thank my parents, who patiently supported me during my whole studies of physics and my girlfriend, who provided mental support and was always interested in my research.

Contents

CHAPTER 1

Introduction

In the Standard Model of particle physics, which describes the fundamental interactions and the elementary particles, many processes have been studied and were confirmed by precise measurements, proving its success. With the currently largest experiments in particle physics, the Large Hadron Collider (LHC), which collides protons at large energies, physicists are able to increase the precision of past measurements, as well as finding new processes not accessible before, due to limited energy scales. As such the coupling of the top quark to the photon is also a quantity, which is predicted by the Standard Model and can be measured with the help of the ATLAS detector that is located at the LHC.

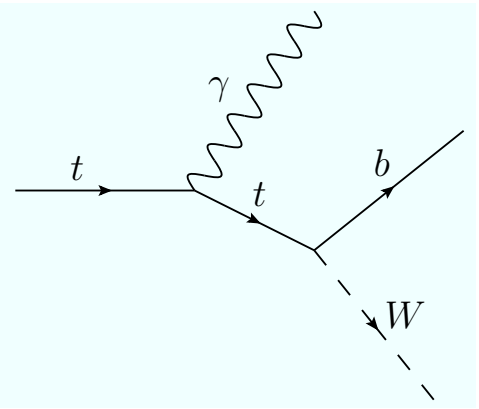

Figure 1.1: Diagram of a photon emission from a top quark.

Figure 1.1 shows the diagram of a top quark emitting a photon and then decaying to a W boson and a b quark. Since the photon couples to charged particles, the top quark is able to radiate it. However many other charged particles are involved in proton collisions, that can also radiate photons. Therefore any study of the $t\bar{t}\gamma$ process involves finding the signal photons (radiated from top quarks) among the background photons (any other photons). This thesis includes two studies for proton collisions at a centre-of-mass-energy of 8 TeV.

- The first study, done at truth level, compares different Monte Carlo generators, which are used for simulating physics processes at high energies, to find the most suitable for the next $t\bar{t}\gamma$ analysis within the ATLAS collaboration. This study is done in the single lepton $t\bar{t}\gamma$ channel
- The second study is a measurement of the $t\bar{t}\gamma$ cross section using events collected at 8 TeV by the ATLAS detector, in the dilepton $t\bar{t}\gamma$ channel. So far no measurements with this channel have been published by any experiment.

CHAPTER 2

Theoretical introduction and experimental setup

The purpose of this chapter is to give a theoretical background for this thesis as well as to introduce the setup of the ATLAS experiment.

2.1 The Standard Model

The Standard Model (called SM in the following) is a theory which describes the elementary particles and the interactions between them. Most of the information in this chapter was obtained from Reference [1].
The particle interactions described by the SM are the strong, the weak and the electromagnetic interaction. They are mediated by the gauge bosons (with spin 1). Additionally the SM describes the fermions (with spin $\frac{1}{2}$) as matter particles, undergoing these interactions. Together with the recently discovered Higgs boson, the particle content of the SM can be classified in three groups:

Gauge bosons

In the SM the interactions between the particles are described as exchanges of (virtual) gauge bosons. The strength of each interaction is described by the corresponding coupling α, which depends on the energy scale. For the energy scales of high energy physics experiments, the strong interaction is the strongest, followed by the electromagnetic interaction, while the weak interaction is the weakest.

Interaction	Gauge bosons	Symbol	Mass [TeV]
Strong interaction	8 gluons	g	0
Weak interaction	W^+ boson	W^+	80.4 [1]
	W^- boson	W^-	80.4 [1]
	Z boson	Z^0	91.2 [1]
Electromagnetic	Photon	γ	0

Table 2.1: Summary of the interactions and the gauge bosons in the SM.

Table 2.1 summarizes the interactions and the gauge bosons in the SM. Each interaction has its unique properties:

- The electromagnetic interaction is mediated by the photon. The photon only couples to charged particles although it carries no charge itself. Additionally it has no mass and is a stable particle.

The electromagnetic interaction is known for a very long time, since its effects can be observed macroscopically as well, for example with magnets or currents. It is responsible for keeping the shell of atoms (consisting of electrons) near the nucleus (consisting of protons and neutrons).

- The strong interaction is mediated by the gluon. Similar to the photon, the gluon is massless and couples to the strong charge, which is called color. The gluon however carries color itself and due to the number of color charges (3 colors and 3 anticolors) and the SU(3) symmetry group of quarks, described by QCD, 8 gluons exist. The strong interaction is responsible for nuclei to be bound and for the formation of jets after collisions of particles.

- The weak interaction is mediated by the charged W boson or the neutral Z boson, which are the only massive gauge bosons. It is responsible for flavor changing decays of quarks, like the beta decay and is the only interaction, which can violate charge-parity (CP) conservation.

Fermions

The SM includes twelve elementary particles which are affected by the interactions. They are further divided into quarks and leptons, depending on whether they are affected by the strong interaction.

Family	Name	Symbol	Charge [e]	Mass [MeV]
1	up quark	u	2/3	2.3 [1]
	down quark	d	-1/3	4.8 [1]
2	charm quark	c	2/3	$1.28 \cdot 10^3$ [1]
	strange quark	s	-1/3	95 [1]
3	top quark	t	2/3	$173.34 \cdot 10^3$ [2]
	bottom quark	b	-1/3	$4.18 \cdot 10^3$ [1]

Table 2.2: Summary of the quarks in the SM.

Table 2.2 summarizes the properties of the quarks. The quarks are affected by all interactions described by the SM. They are organized in families in pairs of an up-type quark and a down-type quark, with each up-type/down-type quark having the same charge. The heavy quarks (of the third generation) are short-lived and decay quickly to lighter quarks of the second and first families.

Family	Name	Symbol	Charge [e]	Mass [MeV]
1	electron neutrino	ν_e	0	0
	electron	e	-1	0.511 [1]
2	muon neutrino	ν_μ	0	0
	muon	μ	-1	105.66 [1]
3	tauon neutrino	ν_τ	0	0
	tauon	τ	-1	$1.78 \cdot 10^3$ [1]

Table 2.3: Summary of the leptons in the SM.

Table 2.3 summarizes the properties of the leptons. Leptons can be further divided into pairs of a charged lepton and the corresponding neutrino. Neither are affected by the strong interaction. The neutrinos are also not affected by the electromagnetic interaction, which makes it hard to detect them in an experiment.

The Higgs boson

The Higgs boson was the most recent discovered elementary particle of the SM. It was predicted to explain the masses of the heavy gauge bosons (W and Z), as well as the masses of the other elementary particles in 1964 [3, 4]. Within the corresponding theory of the Higgs mechanism, the mass of each elementary particle is proportional to the strength of the interaction with the Higgs field. Since the Higgs field is expected to have a carrier, the Higgs boson was postulated, which was searched for intensively for more than 50 years until it was discovered at the LHC by ATLAS [5] and CMS[6] in 2012.

2.1.1 Problems of the SM

Despite the success of the SM in correctly predicting new phenomena like the existence of the top quark or the Higgs boson and describing the experimental data, it cannot explain certain problems in physics. The following list shows some of the major examples not explained by the SM:

- unification of forces:
  As mentioned in Section 2.1, the strength of the interactions described by the SM depend on the energy scale. At which scale the forces have the same coupling strength, if at all, is not answered by the SM. Additionally, at energy scales available at experiments, gravity is multiple magnitudes weaker than the other forces.

- neutrino masses:
  The neutrinos are massless in the SM. However multiple experiments confirmed the existence of neutrino oscillations [7, 8], which cannot be explained with massless neutrinos.

- dark matter:
  To explain the radial velocity of galaxies observed in astronomy, dark matter was postulated, because the mass needed to justify observed velocities, can not be explained by either visible objects in these galaxies or elementary particles in the SM.

Therefore the SM is not complete and many possible extensions have been formulated. It is possible that new physics (not described by the SM) can be seen with the LHC.

2.1.2 The top quark

Since the topic of this thesis is the $t\bar{t}\gamma$ process, the properties and decay channels of the top quark are important. It was discovered in 1995 at the Tevatron collider [9, 10] and it is the heaviest elementary particle within the SM with a mass of 173.34 ± 0.76 GeV [2]. The huge mass is the cause of its short lifetime ($\sim 10^{-25}$ s), which makes the top quark unique, because it is not able to form hadrons before it decays, since the time scale of the strong interaction is a magnitude lower ($\sim 10^{-24}$ s). To measure a top quark, the decay products have to be identified and the top quark needs to be reconstructed.

Production

The top quark is most commonly produced in a $t\bar{t}$ pair. The production of the $t\bar{t}$ pair proceeds via gluon fusion or quark annihilation as shown in Figure 2.1. The relative fractions of the production processes depend on the centre-of-mass energy. At the LHC, the relative fraction of gluon fusion is more than 80%. At the Tevatron with collisions at lower centre-of-mass energy than the LHC and colliding $p\bar{p}$ instead of pp, this fraction is reversed.

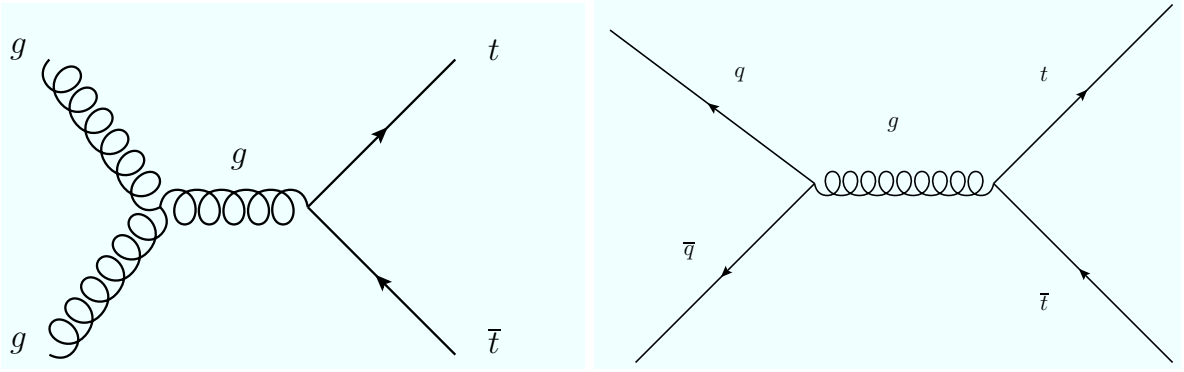

(a) Gluon fusion. (b) Quark annihilation.

Figure 2.1: Sample production diagrams of the $t\bar{t}$ pair.

Figure 2.1 shows two sample production diagrams for a $t\bar{t}$ pair. In addition to the pair production, a single top quark can also be produced via the weak interaction, which is less likely for proton-proton collisions.

Decay

The top quark almost exclusively decays into a W boson and a b quark, with other possible decays substituting the b quark with lighter down-type quarks instead [1]. Any other channel is heavily suppressed. The b quark forms a jet and hadronizes in the detector, while the W boson decays further into either a pair of charged lepton and neutrino ((32.20±0.24)%) or a $q\bar{q}$ pair ((67.41±0.27)%) [1].
Since the most common production of the top quark is via a $t\bar{t}$ pair, the decay channel is most often quoted for the whole pair, depending on how the two W bosons decay. The channels are called fully hadronic (both W bosons decay hadronically), single lepton (exactly one W boson decays leptonically) and dilepon (both W boson decay leptonically) channel. Each hadronic W boson decay adds two more jets to the event. Since the QCD multijet production has a large production cross section at the LHC, the jets provide worse discrimination against the non-top background than the leptons. Therefore the dilepton channel has the cleanest signature, although the branching ratio is also the smallest.

$t\bar{t}$ channel	Number of jets	Number of charged leptons
fully hadronic	6	0
single lepton	4	1
dilepton	2	2

Table 2.4: Properties of the $t\bar{t}$ decay channels.

Table 2.4 summarizes the properties of the $t\bar{t}$ decay channels. The corresponding branching ratios can be calculated with the branching ratios from the W decays. The branching ratios for $t\bar{t}$ are 44% for the fully hadronic, 44% for the single lepton and 11% for the dilepton channel. These numbers include $W \to \tau\nu$. However those are often not considered, but the decay products of the τ lepton are added to the appropriate channels instead, e.g. in case of $\tau \to e\nu$ the decay is added to the leptonic channels.

Figure 2.2 shows the diagram of the $t\bar{t}$ dilepton decay channel.

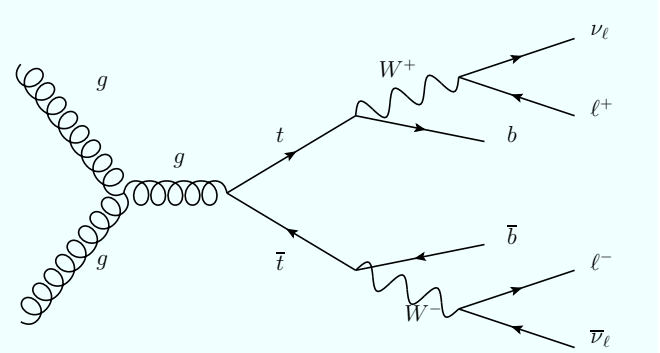

Figure 2.2: Diagram of the $t\bar{t}$ dilepton channel.

2.2 The ATLAS experiment

ATLAS (A Toroidal LHC ApparatuS) is an experiment, which is located at the the particle accelerator LHC (Large Hadron Collider).

2.2.1 The Large Hadron Collider

The LHC is a circular proton accelerator located at CERN, the "European Organization for Nuclear Research" near Geneva at the Swiss-French border. It has a circumference of roughly 27 km and is the largest accelerator of its kind, collecting data since 2010. From 2010-2011 the accelerator ran at 7 TeV and delivered 47 pb^{-1} and 5.5 fb^{-1} of proton-proton collisions in 2010 and 2011 [11]. The accelerator was upgraded to run at 8 TeV afterwards, started running again in 2012 and delivered more than 20 fb^{-1} of data. In the following years the LHC was upgraded to run at 13 TeV and just completed a run in 2015. The accelerator was built beneath the earth to shield the experiments from radiation above the ground. There are 4 main experiments stationed at the LHC, which are ATLAS [12], CMS (Compact Muon Solenoid) [13], ALICE (A Large Ion Collider Experiment) [14] and LHCb (Large Hadron Collider beauty) [15].

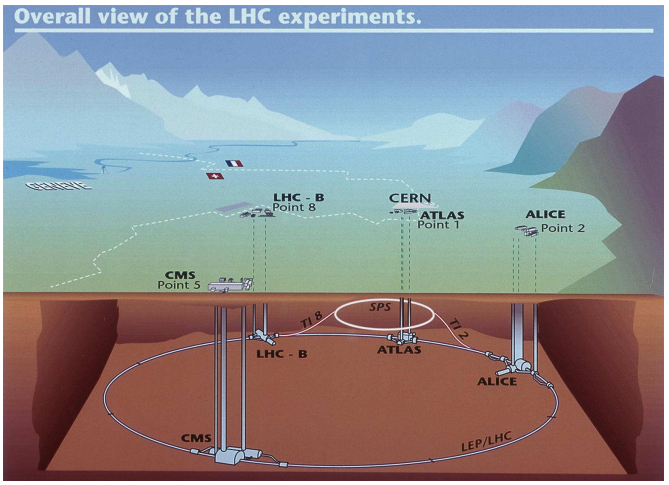

Figure 2.3: Location of the LHC and its experiments (© CERN).

Figure 2.3 shows the layout of the LHC and its experiments. Together with CMS and LHCb, the

ATLAS experiment is investigating proton-proton collisions, whereas ALICE focuses on heavy ion collisions. While ATLAS and CMS surround nearly the entire solid angle around the collision point, the LHCb detector only detects in the forward direction and specializes on b-quark physics. ATLAS and CMS study the whole range of Standard Model physics and aim at finding new physics.

2.2.2 The ATLAS detector

The ATLAS experiment is the largest detector of the 4 main experiments at the LHC with a length of 44 m and a height of 25 m. The overall appearance of the detector is a cylindrical form and like many detectors at particle accelerator it consists of many subdetectors distributed in onion-like layers.

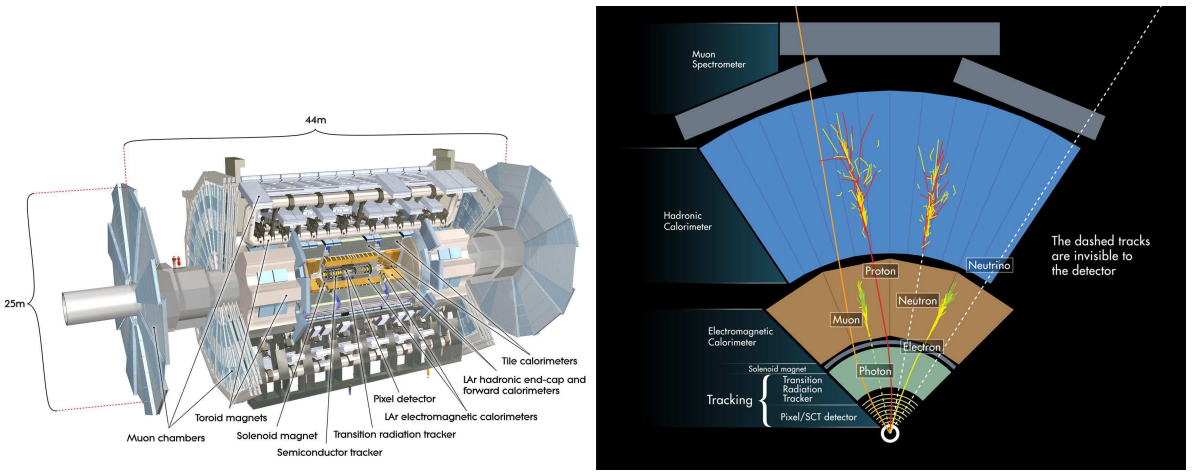

(a) Appearance of ATLAS (© CERN). (b) Schematic view of ATLAS (© CERN).

Figure 2.4: Appearance and structure of the ATLAS detector.

Figure 2.4 shows the appearance of the detector (see Figure 2.4a) and the distribution of the subdetectors (see Figure 2.4b). The main subdetectors of ATLAS are:

- The inner detector
- The electromagnetic and hadronic calorimeters
- The muon spectrometer

The inner detector

The inner detector is very close to and surrounds the beam pipe of the accelerator. It follows the cylindrical shape of the whole ATLAS detector and a magnetic field of 2 T is used to bend the charged particles produced in the collisions. The field enables the experiment to estimate the momenta and charges of the particles and reconstruct their tracks. The inner detector has a substructure of three detectors:

- The pixel detector:
  The innermost detector is made of 1744 silicon pixel modules. The size of each pixel is in the range of μm^2 and they are arranged in three cylindrical layers and two endcaps around the beam pipe. This setup allows for three hits per track, caused by a charged particle.

- The semiconductor tracker (SCT):
  The SCT adds four layers of silicon detectors on top of the three pixel layers from the pixel detector. The size of each is in the range of cm^2 and each detector contains 768 strips instead of pixel modules. The larger surface of each detector allows to extend the measurement of tracks from charged particles.

- The transition radiation tracker (TRT):
  Tubes of 4 mm diameter are placed on the outer part of the inner detector. The tubes are filled with Xenon gas, which allows the TRT to be the innermost detector to distinguish electrons from hadrons, because of the interaction of electrons and the Xenon gas. The tubes are arranged in modules, with each module containing hundreds of tubes. Due to the large number of modules, the TRT registers more than 20 hits per track of a charged particle.

The electromagnetic and hadronic calorimeters

ATLAS uses two calorimeters. Due to the different Bethe-Bloch profile of each particle, most electrons and photons deposit their energy in the electromagnetic calorimeter, while hadrons deposit their energy in the hadronic calorimeter. The deposited energy and the position can be measured in the segmented calorimeters.

- The electromagnetic calorimeter:
  In the innermost calorimeter electrons lose their energy due to bremsstrahlung, while photons lose their energy by creating electron-positron pairs. The combination of these processes creates electromagnetic showers. The material of the calorimeter absorbs these showers and the energy of the particles is deposited in the material. The electromagnetic calorimeter stops electrons and photons, while hadrons only deposit a fraction of their energy in it.

- The hadronic calorimeter:
  The other calorimeter works very similar to the electromagnetic calorimeter, but has to be much larger. Hadrons do not produce electromagnetic showers, but hadronic showers and travel over a longer distance. To avoid hadrons from passing beyond the hadronic calorimeter, the thickness of the material is increased, in comparison to the electromagnetic calorimeter.

The muon spectrometer

Of the particles with a long lifetime, Muons are not be stopped in the calorimeters unlike pions and kaons which lose their energies in the hadronic calorimeters. Fortunately muons are the only detectable elementary particles which are able to pass both calorimeters (neutrinos can not be detected). The muon spectrometer is the largest part of ATLAS and is placed on the outermost part of the detector. Similar to the inner detector a magnetic field is used to determine the trajectory, momentum and charge of the muon. Since only muons are detected in the muon spectrometer, tracks from muons are reconstructed with more than 98% efficiency, while electrons and hadrons are reconstructed with 70-95% efficiency in the ATLAS detector.

2.2.3 The trigger system

The collisions happen at a high rate at the interaction point in the ATLAS detector. It is not possible to store data from every collision, because the amount of collisions is magnitudes higher than the capability

of storing the information for every event. Fortunately not every collision results in a physics process of interest. Thus a trigger system is required to distinguish interesting from disposable events. In ATLAS the trigger system categorizes events in three levels.

- Level-1 (L1):
  The L1 trigger uses only a part of the subdetectors from ATLAS. Muons with large transverse momentum are sought with the muon spectrometer and the calorimeters search for electrons, photons and jets with large transverse momentum. Also high amounts of missing transverse energy $E_{\mathrm{T}}^{\mathrm{miss}}$ are of interest in the calorimeters.
- Level-2 (L2):
  After passing the L1 trigger the L2 trigger identifies position, energies and transverse momenta. The event is then compared to signatures of processes of interest.
- Event filter (EF):
  The EF applies an event selection to the remaining events, based on the signatures determined by the L2 trigger.

The collision rate at the ATLAS detector is in the range of MHz and is reduced to less than 1 kHz by the trigger system.

2.2.4 The coordinate system of ATLAS

ATLAS commonly uses the coordinates η, ϕ and z with the collision point at the origin. The z-axis corresponds to the beam axis, while x points to the center of the accelerator and y points upwards. The positive z direction is defined such, that the coordinate system becomes right handed. Due to the shape of the ATLAS detector, cylindrical coordinates are used in the (x, y)-plane. The angle ϕ is the azimuthal angle around the beam pipe and instead of using the polar angle θ, it is more common to use the pseudorapidity η defined as

$$\eta = -\ln\left(\tan\frac{\theta}{2}\right) = \frac{1}{2}\ln\left(\frac{p + p_z}{p - p_z}\right) \tag{2.1}$$

Equation 2.1 shows the definition of the pseudorapidity η. The pseudorapidity can be expressed in terms of the momentum of a particle and the difference of two pseudorapidities are Lorentz invariant.

$$\Delta R = \sqrt{\Delta\phi^2 + \Delta\eta^2} \tag{2.2}$$

Equation 2.2 shows the definition of ΔR, which is used to denote the distance of two objects in the (ϕ, η)-plane. The ΔR of two objects is Lorentz invariant to the boosts along the beam direction.

2.3 Monte Carlo simulation

Monte Carlo (MC in the following) generators are computer programs used to simulate the high-energy collisions. Together with the simulation of the detector they provide predictions of the detector response to the collisions events. They are used in the design of new detectors and experiments as well as in the experimental data analysis. The generators provide predictions that are tested by the experiments. Some parameters of the models they use can be adjusted such that the generator predictions describe the collisions data. Therefore the use of MC is interesting for both theory and experiments in physics.

The information in this section relies on Reference [16]. In the example of high energy physics at the LHC, proton-proton collisions are simulated by MC event generators. In order to simulate such a collision, most MC event generators split the simulation in multiple parts. The hard process describes the interactions between the two partons (constituents of the proton) that happens at a high energy scale (Q^2 in Figure 2.5). It sets the initial conditions for the parton shower (defined below). The partons participating in the hard event originate from the colliding hadrons. The Parton Distribution Function (PDF in the following) is defined as a probability density f for finding a particle with the fraction x of the longitudinal momentum of the hadron, when the hadron is probed at the resolution scale of Q^2.

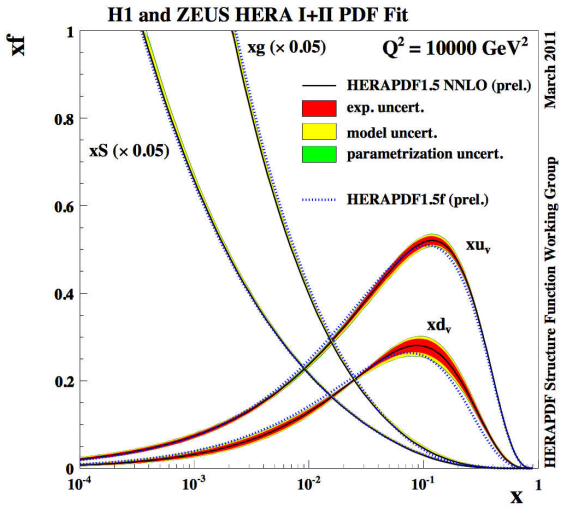

Figure 2.5: PDF distributions f for different partons at $Q^2 = 10000\ \text{GeV}^2$ as a function of the parton longitudinal momentum fraction x [17].

Figure 2.5 shows the longitudinal momentum fraction x times the PDF distribution f for the partons inside a proton as a function of x. The shown momentum transfer is at $Q = 100\ \text{GeV}$, which is an appropriate order of magnitude for the LHC. Due to their huge contribution, the PDFs of the gluon and the sea-quarks are scaled down for better visibility. This distribution shows that events with small fraction of x are much more likely. Also, the production process for this kind of events will be mostly gluon gluon fusion instead of quark annihilation, which is important also for the $t\bar{t}$ event production at the LHC, as mentioned in Section 2.1.2. The most important parts of a MC simulation are summarized in the following:

- The hard process:
  The hard process describes the physics process of interest. For example if a MC models $t\bar{t}$ events, the whole channel including top decays and the decays of the two W bosons are part of the hard process. Figure 2.2 is an example of a hard process for the dilepton channel of $t\bar{t}$. Since the hard process takes place at a high energy scale where the QCD coupling is weak, perturbative calculations can be used. In the hard process the partons remain free, since the hadronization takes place at lower energy scales at which the QCD coupling becomes large. The hard process is also sometimes referred to as the matrix element.

- The parton shower:
  The partons inside the protons before the collision are mainly affected by the strong interaction. During the collision the partons radiate gluons because of their color charge. This includes the

gluon itself which carries a color charge as well. Similar to QED radiation, a shower is produced by the partons according to QCD. This is called the parton shower. It is simulated in steps, starting from the highest momentum transfer, continuing to smaller momentum transfers until the low momentum scale at which the non-perturbative effects become dominant.

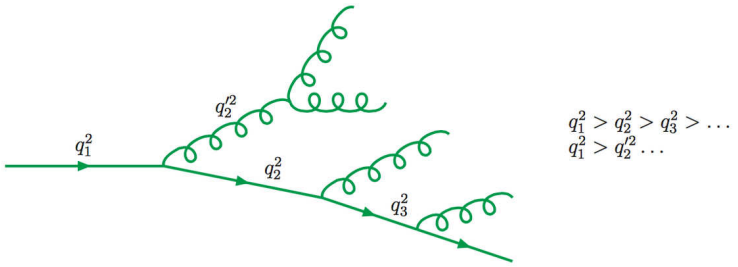

Figure 2.6: A parton shower with decreasing momentum transfers [16].

Figure 2.6 shows how the momentum transfer in a parton shower is decreasing after multiple interactions.

- The hadronization:
  The SM requires color charged objects to be confined. Therefore each object radiated in a parton shower needs to hadronize at some point. This is done by the hadronization process and handled by certain models in the simulation.

- The underlying event:
  Initially the proton is a color neutral object. In a collision where a parton is effectively "removed from the proton", the remnants are not color neutral anymore, so they have to produce a parton shower and hadronize, too. Further collisions between the partons of the two protons can occur. This however is only secondary in the event, since the highest momentum was transferred with the parton initially removed from the proton. It is called the underlying event and usually involves partons and hadrons of very low momenta (soft).

- Unstable hadron decays:
  The hadrons produced by the hadronization in the primary and underlying event are not necessarily stable particles. If a resonance or a meson containing quarks of higher generations is produced, it will further decay until a stable hadron is formed. This is the last step handled by the simulation.

The stages of the event generation described above can be shared among different MC generators. For example if a Powheg + Pythia $t\bar{t}$ MC is quoted, the hard process was modeled using Powheg [18], while the parton shower, underlying event and the hadronization was modeled by Pythia [19].

2.3.1 Order of precision

Since this thesis puts an emphasis on samples being calculated at leading-order (LO) or next-to-leading-order (NLO), an understanding of these terms is essential. These terms describe theoretical calculations of matrix elements in physics processes. A typical LO diagram is shown in Figure 2.1, which illustrates the production of a $t\bar{t}$ pair via either gluon fusion or quark annihilation.

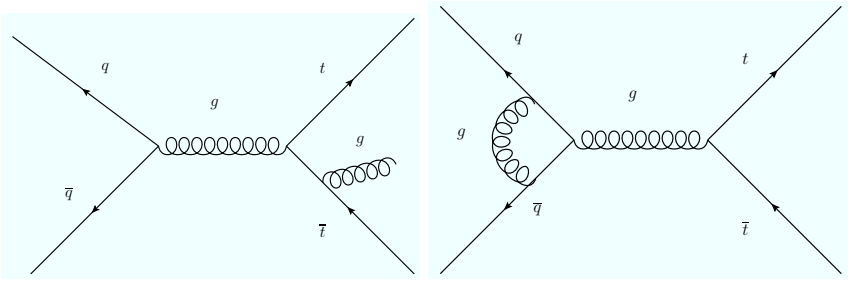

(a) Extra real emission. (b) Extra loop.

Figure 2.7: QCD NLO diagrams for the production of a $t\bar{t}$ pair via quark annihilation.

Figure 2.7 shows two possible NLO diagrams for the $t\bar{t}$ pair production via quark annihilation. NLO diagrams, as defined for the purpose of this thesis feature one of two possible additions to the LO diagram:

- An extra emission, like in Figure 2.7a.
- An extra loop, like in Figure 2.7b.

The example diagrams show NLO in QCD, which means that only one extra gluon emission or loop is allowed. There are many additional NLO diagrams in QCD for the example of the $t\bar{t}$ pair production via quark annihilation, which makes the calculation of all of them involved.

CHAPTER 3

Monte Carlo simulation studies

3.1 Introducing the samples

As mentioned previously, the motivation for Monte Carlo simulation studies is to find the MC event generator that describes the $t\bar{t}\gamma$ process the best and to identify the phase-space regions, that have enhanced sensitivity to the $t\bar{t}\gamma$ coupling. In order to study this, all $t\bar{t}\gamma$ samples are separated in one of two kinds, following the convention of Reference [20]:

- **production samples**: these samples consist of $t\bar{t}$ events with at least an additional photon, coupled to either the initial state or the top quarks themselves. Photons radiated from the top decay products in the matrix element final state are not allowed. These kind of events are simulated by using an additional event generator modeling the QED radiation. The top and anti-top quarks decay non radiatively in the hard process ($pp \to t\bar{t}\gamma$), which means this sample does not have photons radiated from the final state in the hard process.

- **decay samples**: these samples have no constraints on where the photon can be radiated from, so radiative top decays are allowed. This is in addition to all processes of the production samples, so the decay samples include both $pp \to t\bar{t}\gamma$ and $t \to bW\gamma$.

Additionally, this study uses $t\bar{t}$ samples to compare to invariant mass distributions of the $t\bar{t}\gamma$ samples. The categorization of production and decay samples is relevant because the contribution of radiative top decays is not negligible, even for photons with high p_{T}.

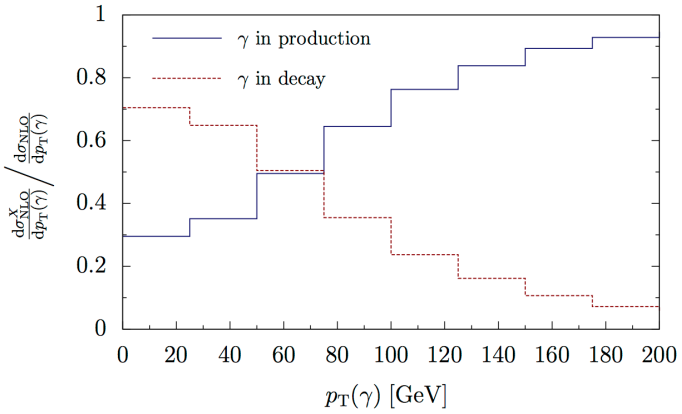

Figure 3.1: Fraction of photon radiation in production and in decay $(pp \to t\bar{t}\gamma)/(t \to bW\gamma)$ [21].

Figure 3.1 shows the p_{T} distribution of photons radiated in the production in comparison to photons radiated in the decay. The ratio on the vertical axis corresponds to fraction of events, while the ratio in the caption of the figure corresponds to events with photons radiated from either the initial state or a top quark (production) divided by events with photons radiated in the final state (decay). The samples shown in Figure 3.1 were computed at NLO in QCD with a renormalization and factorization scale at the top mass (m_t = 172 GeV) [21]. As expected, the photons radiated in the decay are softer than those radiated in the production, however even photons above 150 GeV are radiated in the decay at a non negligible rate.

Allowing photons to be radiated from the decay products of the top quark includes more Feynman diagrams, since the number of particles from which the photon can be radiated from is increased. This increase of Feynman diagrams can be seen in the distribution of the PDF (see Section 2.3) for the two samples.

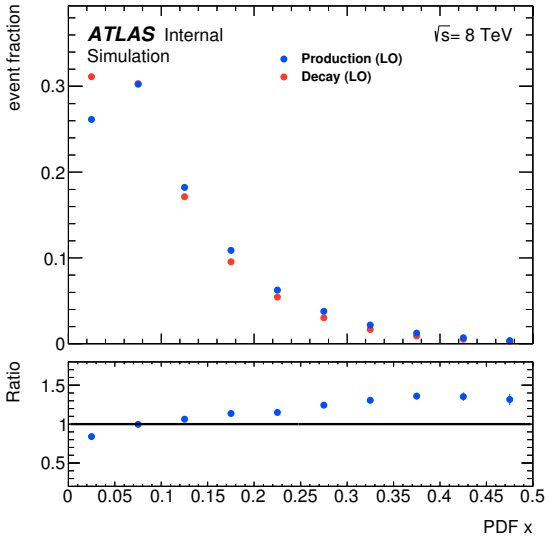

Figure 3.2: PDF distribution comparing $t\bar{t}\gamma$ production and decay sample.

Figure 3.2 shows the PDF distribution for both the production and decay samples at LO for the incoming partons participating in the collision and yielding a $t\bar{t}\gamma$ event. For small values of x, the samples contribute differently; the decay sample has an excess. In collisions two $t\bar{t}\gamma$ productions at LO are possible: the gluon fusion and the quark annihilation. The latter one involves quarks, which allows for photon radiation. The fraction of the two different production processes can be examined by looking at the PDG-ID information for the initial process. The PDG-ID is the Monte Carlo numbering scheme maintained by the Particle Data group [1]. When using MC samples, it is possible to ask for each particle involved in an event, by accessing the PDG-ID values. Each particle has its own PDG-ID number:

- quarks: 1-6
- leptons: 11-16
- gauge bosons: 21-24

Antiparticles get the corresponding negative number. The gaps 7-10 and 17-20 are not used and reserved for additional quark and lepton generations. The PDG-ID values are only accessible in simulation samples, since in real data particles have to be reconstructed by the detector.
Since there is only one photon allowed in the hard process for the leading order samples, the addition of Feynman diagrams with photons radiated from the top decay products change the relative fraction of initial state radiation to final state radiation. This fraction will also affect the relative fraction of gluon fusion and quark annihilation.

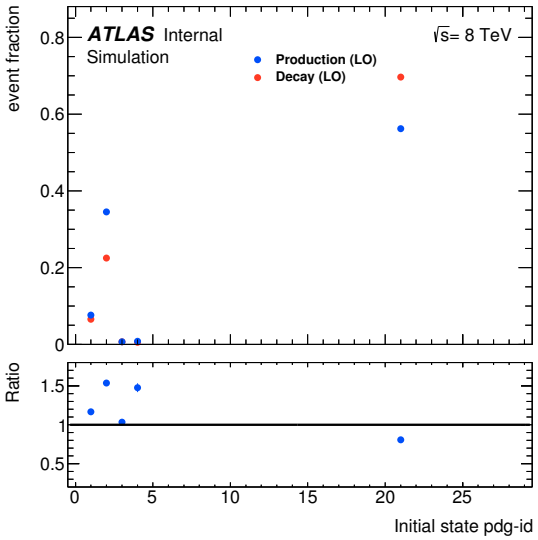

Figure 3.3: PDG-ID of the initial process.

Figure 3.3 shows the fraction of each particle involved in the initial process. As expected only two kinds of particles contribute: gluons (PDG-ID = 21) and light quarks (PDG-ID = $\{1, 2, 3, 4\}$). Using the fractions for each particle in the histogram, the contribution for both processes can be calculated for each sample.

	production sample	decay sample
gluon fusion	0.563	0.697
quark annihilation	0.437	0.303

Table 3.1: Fractions for both $t\bar{t}\gamma$ production processes in the two samples.

Table 3.1 shows the numbers for both $t\bar{t}\gamma$ production processes. The production via quark annihilation is more likely in the production samples than in the decay samples. This enhances the contribution of initial state radiation, because the photon cannot be radiated in the initial state for the gluon fusion process.

3.1.1 Order of precision

If possible it would be preferable to use decay samples, because they are expected to resembles nature the best. However the order of precision also matters. The decay samples allow for more Feynman

diagrams, because the number of possible particles the photon can be radiated from, is increased. However they are more difficult to compute because of the increased number of diagrams. For LO, both the production and decay samples are available, but already at the NLO the decay samples are too complex to be computed. Therefore in the following, decay samples at LO, which are able to have decayed top quarks in the matrix element final state, with the addition of photons and the production samples at NLO, which provide better modeling, while not having decayed top quarks with additional photons in the matrix element final state will be compared. In order to find an answer, which one describes the $t\bar{t}\gamma$ signal process better, a few conditions have to be defined for these samples. For the 7 TeV $t\bar{t}\gamma$ measurement at ATLAS [22] and the 8 TeV $t\bar{t}\gamma$ measurement at CMS [23] LO generators were used. In both measurements radiative top decays in the hard process were allowed, defined like the decay samples. The measurements used shapes from the MC simulations and normalization from the theoretical predictions.

- The QED radiation should be able to provide a good description of high-p_{T} photon emissions from the top decay products (production samples).

- The contribution of the extra Feynman diagrams in the case of decayed top quarks in the matrix element final state (decay samples) with additional photons should be small.

Both these conditions have to be fulfilled in order for the NLO production samples to be preferred. For the first condition, the photons radiated by the top decay products will be handled by QED generators like Photos [24] in the case of the production samples. This condition can be tested by a direct comparison of the photon p_{T} distributions, since both are using Photos. For the second condition, the additional Feynman diagrams for the decay samples should not affect kinematic quantities of the photon too much. If any of these conditions fail, the decay samples at LO will be preferred as the better $t\bar{t}\gamma$ event description.

3.1.2 Settings

The purpose of this Section is to describe the settings of all samples used in this MC analysis.

Three $t\bar{t}\gamma$ samples are compared: the LO production, the LO decay and the NLO production sample. Additionally a NLO $t\bar{t}$ sample will be used for reference but is not taken into consideration for a choice of the $t\bar{t}\gamma$ simulation. A few technical settings of these samples are important to justify a comparison.

For the LO samples the event generation is handled by MadGraph [25], which includes the parton distributions and the hard process part of the event generation. The showering and hadronization generator used is Pythia6 [19] and the QED radiation is handled by Photos. The renormalization and factorization scale is set to twice the top mass of 172.5 GeV. These settings apply to both LO samples, which allows for a good comparison.

For the NLO samples the event generation is done differently. The PowHel package [26] is used to compute these samples. This package consists of a tool to calculate the QCD predictions at NLO precision (Helac-NLO [27]) and a tool to simulate the events at multiple stages of the event generation (Powheg-BOX [18]). The showering and hadronization generator and the QED radiation generator are the same as for the LO samples, namely Pythia6 and Photos. However the renormalization and factorization scale is dynamic and set to half of the transverse mass of the final state particles.

In order to obtain MC predictions, several quantities need to be set, such as the hard process scale or parameters of the models used to describe the process for which non-pertubative calculations are needed.

NLO $t\bar{t}$

The $t\bar{t}$ sample is used as a comparison to the $t\bar{t}\gamma$ samples in this Chapter. It is generated using Powheg-BOX for the hard process at NLO precision and Pythia6 for the parton showering and the underlying event. The NLO $t\bar{t}$ sample uses a fixed renormalization and factorization scale.

$$Q = \sqrt{m_t^2 + p_{\mathrm{T}}^2} \tag{3.1}$$

Equation 3.1 shows the scale choice for the NLO $t\bar{t}$ sample, with m_t and p_{T} being the mass and the transverse momentum of the top quark.
The version of the generator for the hard process is Powheg-BOX version 1, release 2129 with the PDF CT10, the version of the parton shower generator is Pythia 6.4.26 with the PDF CTEQ6L1 and the Perugia 2011C tune [28].

NLO $t\bar{t}\gamma$ production

The NLO $t\bar{t}\gamma$ production sample is used in comparison to the LO production samples in this Chapter. It is generated using PowHel for the hard process at NLO precision, Pythia6 for the parton showering and Photos for the QED radiation. This sample is designed to have exactly one photon in the matrix element final state, while the photon radiations of the decay products of the top quarks are not handled by the matrix element calculation, but rather left to Photos.

The NLO $t\bar{t}\gamma$ sample use a dynamic renormalization and factorization scale.

$$Q = \frac{1}{2}\left(m_{\mathrm{T,t}} + m_{\mathrm{T},\bar{\mathrm{t}}} + p_{\mathrm{T},\gamma}\right) \tag{3.2}$$

Equation 3.2 shows the definition of the hard process scale, which is used for the renormalization and factorization scale μ in the NLO samples. It is defined as half the sum of the transverse masses of the final state particles. The definition of the transverse mass is similar to the definition of the mass:

$$m^2 = E^2 + p^2 \rightarrow m_{\mathrm{T}}^2 = E^2 + p_{\mathrm{T}}^2$$

For the hard process the PDF CT10nlo was used, for the parton shower Pythia 6.4.25 was used with the PDF CTEQ6L1 and the Perugia 2011C tune [26]. Since this is a $t\bar{t}\gamma$ sample, the QED emission has to be handled as well, which is done by Photos.
When using this sample, the phase-space cuts need to be mentioned as well. The sample contains only events with one W boson decaying into a $q\bar{q}$ pair and the other W boson decaying into a lepton and neutrino pair. The photon is required to have at least a p_{T} of 30 GeV. This requirement is important when using other samples to compare, because the LO samples allow much softer photons in general. Whenever using the NLO $t\bar{t}\gamma$ sample for comparison, the corresponding cut of the p_{T} of the photon needs to be set to 30 GeV for the other samples as well. There are multiple samples available with the settings described, which differ in the isolation of the photons. The isolation of the photons is defined as:

$$E_{\perp,had} = \sum_i E_{\perp,i} \cdot \theta(R_\gamma - R(p_\gamma, p_i)) < E_{\perp,had}^{max} \tag{3.3}$$

Equation 3.3 shows the total hadronic transverse energy $E_{\perp,had}$, in terms of the photon cone size R_γ. The cone is defined as a half opening angle with a given value, around the direction of the corresponding

object. Inside this cone, all reconstructed energies are attributed to the object. The sum is over all partons in the event and $R(p_\gamma, p_i)$ is the distance of the photon and the corresponding parton. For the measured quantities the index i would refer to the tracks instead of the partons. $E^{max}_{\perp,had}$ is the maximal hadronic energy allowed in the cone of R_γ. The sample used in this thesis has a value of $R(p_\gamma, p_i) = 0.05$.

LO $t\bar{t}\gamma$ production and $t\bar{t}\gamma$ decay

Dedicated LO $t\bar{t}\gamma$ samples were produced for this thesis using MadGraph. The MadGraph card, which contains the complete information regarding all settings can be found in the Appendix A.1.1. The most important settings are summarized in this section.

The only difference between the LO $t\bar{t}\gamma$ production and decay samples is the definition of the hard process. For the production, the photon cannot be radiated from the top decay products in the hard process, while for the decay it can.

- Processes common to the production and decay samples:

```
p p > t t~ a, (t > W+ b, W+ > uc ds~), (t~ > W- b~, W- > l- vl~)
p p > t t~ a, (t > W+ b, W+ > l+ vl), (t~ > W- b~, W- > ds uc~)
p p > t t~ a, (t > W+ b, W+ > l+ vl), (t~ > W- b~, W- > l- vl~)
p p > a (t>(W+>uc~ ds~)b) (t~>(W->l-vl~)b~) a
```

- Processes specific to the decay sample:

```
p p > t t~ > l+ vl  b ds uc~ b~ a
p p > t t~ > uc ds~ b l- vl~ b~ a
p p > t t~ > l+ vl l- vl~ b  b~ a
```

These lines describe the hard process used in the LO samples. Since these lines were taken from the MadGraph card, the particles are described by some uncommon symbols. Antiparticles are described by a tilde, leptons are described by the letter l with the corresponding charge, neutrinos are described by vl and photons are described by the letter a. The first four lines describe the photon emission from either a top quark or the initial state, while the last three lines describe processes with photons radiated from the decay products of the top quark. To simulate the hard process events missing from the production samples, the generator Photos is used for the QED emission.

The version of the generator for the hard process is MadGraph 5.2.1.0 with the PDF CTEQ6L1. The version of the parton shower generator is Pythia 6.4.27 with the PDF CTEQ6L1 and the Perugia 2011 tune (the same as for the NLO samples).

The samples contain single lepton and dilepton $t\bar{t}\gamma$ events , although only the single lepton events are studied here, while the dilepton events are removed in the event selection (see Section 3.2). The p_{T} requirement is 15 GeV for the photon and the lepton. If the LO samples are compared the NLO sample, the photon p_{T} requirement is increased to 30 GeV. Both the photon and lepton $|\eta|$ need to be smaller than 5. The minimum ΔR of the photon to any jet, or the lepton, needs to be at least 0.2. The value of α_{EM} is set to 1/137.

Parton shower generators

This section of the thesis will cover some result obtained with the parton shower generators FORTRAN HERWIG [29] and HERWIG++[30], replacing PYTHIA6.

- FORTRAN HERWIG:
  The version of the generator is 6.520 with the PDF CTEQ6L1 and the AUET2 tune [31].
- HERWIG++:
  The version of the generator is 2.6.3 with the PDF CTEQ6L1 and the UEEE4 tune. Additionally this generator has a very good internal implementation of QED emissions [32] and there are no attempts to try external QED emission generators, since their implementation would be very demanding. The main difference to using PHOTOS for the QED emission is the enhancement of including higher-order corrections for the QED [33].

3.2 Object and event selection

In order to have the correct events selected from data and to test the MC samples, an event selection has been developed. These events should be measurable by the ATLAS detector and emphasize the $t\bar{t}\gamma$ signal events. This will be especially interesting for the decay samples, because the event selection aims at suppressing events with photons radiated from the top decay products. It is expected that the event selection will make the distributions of the production and decay samples more similar, because it removes events in the regions of phase space which are very different. The concrete values for the selection were chosen based on Reference [34] and the 7 TeV $t\bar{t}\gamma$ analysis [22].

3.2.1 Object selection

This part of the selection describes how the physics objects are selected, but does not introduce any requirements to an event. For this categorization the transverse momentum (p_{T}) and the pseudorapidity (η) will be sufficient. The latter observable depends on the detector and will be tuned to allow the best coverage for the ATLAS detector.

- Leptons are required to have at least 25 GeV of transverse momentum.
- Photons are required to have at least 30 GeV of transverse momentum. The choice of using at least 30 GeV for the transverse momentum will result in many neglected photons, radiated from the top decay products, but it is used for better comparison, since all photons of the NLO samples have this requirement applied already in the event generation.
- Jets are required to have at least 25 GeV of transverse momentum.

For all leptons, photons and jets, in addition to the requirement on the transverse momentum, the absolute η should be in the range of 0 to 2.5.

3.2.2 Event selection

This part of the selection is essential for both types of samples (production and decay), since it filters single lepton $t\bar{t}\gamma$ events from the samples, that contain both single lepton and dilepton events. The particles, that will pass this stage of the event selection, will be used further on, while the ones that don't pass will be neglected.

- The number of leptons should be exactly one, to ensure having a single lepton $t\bar{t}\gamma$ event instead of having fully hadronic, dilepton or background events.

- The number of photons should be at least one, allowing multiple photons radiated from particles. There is exactly one photon in the hard process of each sample, however the parton shower and the QED emission are also able to create photons.

- The number of jets (light and b-tagged jets) should be at least four, since a $t\bar{t}\gamma$ event in the single lepton channel is expected to feature at least two light jets and two b-tagged jets (see below). For this specific selection almost all kinds of combinations are allowed as long as there is at least one good b-tagged jet in the event, because the b-tagging efficiency also plays a role (see next Section).

b-tagging

Since the event selection distinguishes between light and b-tagged jets, the term b-tagging has to be defined for the purpose of this Section. The MC samples used for this analysis have a truth record which gives information for each particle, like charge, kinematics and information about the parent particles. Similarly there is a truth record for all jets in the event. The truth record provides information on whether a jet originated from a b-quark or not. If it does, then it is defined as a b-jet, otherwise it is defined as a light jet.
In order to be compatible with a data analysis, there is an additional requirement for a jet to be considered a b-tagged jet: A randomized function recognizes a b-jet as a light jet, with a chance of 30%. The purpose of this function is to simulate the b-tagging efficiency of the ATLAS detector using the best performing algorithm (in terms of b-tagging efficiency) based on a 8 TeV sample [35].
In a data analysis the opposite case has to be taken into account as well. If a light jet is accepted as a b-tagged jet, it adds to the uncertainties of any result. However for this truth analysis the mistag rate, which is defined as fraction of light jets accepted by the b-tagging algorithm over all light jets, is neglected. This mistag rate is estimated to be less than 0.02 for jets with p_{T} lower than 200 GeV [36], hence it is a small effect in comparison to the b-tagging efficiency.

Isolation requirements

This part of the event selection is very important to suppress events with photons radiated from the top decay products. Every particle should be isolated, in order to be identified, without being mixed up with other particles. Only particles which pass the kinematic requirements of the object selection are considered here.

- The ΔR between any two jets has to be at least 0.4, same for each jet and the lepton (this already covers all ΔR values for the decay products).

- The ΔR values of the photons to the $t\bar{t}$ decay products have to be even larger, since the events with photons radiated from the decay products will be removed. The exact values are taken from the corresponding 7 TeV analysis [22].

Table 3.2 summarizes all isolation cuts in the event selection. For the jets and photons all possible combinations are included.

particle	isolation cuts
b-tagged jets	$\Delta R(b, b) > 0.4$
light jets	$\Delta R(j, j) > 0.4$, $\Delta R(j, b) > 0.4$
lepton	$\Delta R(\ell, j) > 0.4$, $\Delta R(\ell, b) > 0.4$
photons	$\Delta R(\gamma, \ell) > 0.7$, $\Delta R(\gamma, j) > 0.5$, $\Delta R(\gamma, b) > 0.5$

Table 3.2: Isolation cuts applied to the samples.

3.3 Results

Most figures in this section will compare two or more histograms. The histograms will not have absolute event numbers shown on the vertical axis, but event fractions, because comparing the shapes of the histograms is sufficient for our purpose. The figures also show a ratio at the bottom. Each ratio is defined as:

$$\text{Ratio} = \frac{\text{color shown}}{\text{color not shown}}$$

Let's consider a figure with two histograms in blue and red: If the ratio part of the figure only shows a red ratio, this ratio was calculated by dividing the values of the red histogram by the values of the blue histogram. Additionally all figures shown in this section have the event selection, presented in Section 3.2, already applied, unless mentioned otherwise.
Most of the Figures show results for stable particles. In MC samples there is a differentiation between stable and hard process particles. Hard process (as discussed in Section 2.3) represents the physics process of interest. An example usage of the hard process is to differentiate single lepton and dilepton events in the MC samples used for this thesis. This can be done by requiring exactly one hard process lepton to remove all dilepton events. On the other hand, stable particles include particles from the parton shower and other stages of the simulation (see Section 2.3. Especially for photons it is necessary to look at stable particles, since the influence of the parton shower and QED emission is studied in the generator comparison (of production and decay). The two kinds of particles can be differentiated in a MC sample by asking for the status code. The status code differs for the type of generator used. For MadGraph samples, this status code is 1 for stable particles and 3 for hard process particles.

3.3.1 Distributions of kinematic observables

In order to compare the samples described in Section 3.1.1, the distributions for kinematic quantities are compared. First the p_{T} distribution of the photon with the highest p_{T} for each event is inspected. An estimate of how many photons are selected per event is also important.

Figure 3.4 shows the stable photon multiplicity. As a reminder, photons with a transverse momentum larger than 30 GeV (and inside the range of $|\eta(\gamma)| < 2.5$) are selected. The majority of the events have only one photon. While the LO samples agree with each other, the NLO samples have a few events with one additional photon more, produced by the QED emission or the parton shower.

Table 3.3 shows the event fractions for the number of photons in the three MC samples. The fractions correspond to Figure 3.4. Only photons that pass the object selection are considered here. For the events with more than one photon, the photon with the highest p_{T} (the hardest photon) is the most likely to have been radiated from the initial state or the top quark as seen in Figure 3.1.

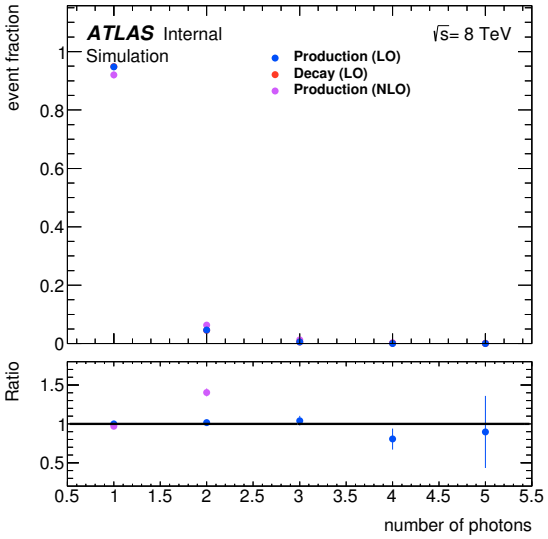

Figure 3.4: Distribution of the photon multiplicity.

Photon multiplicity	LO production	LO decay	NLO production
Exactly one [%]	94.8	94.9	92.0
More than one [%]	5.2	5.1	8.0

Table 3.3: Event fractions for the number of photons in the three samples.

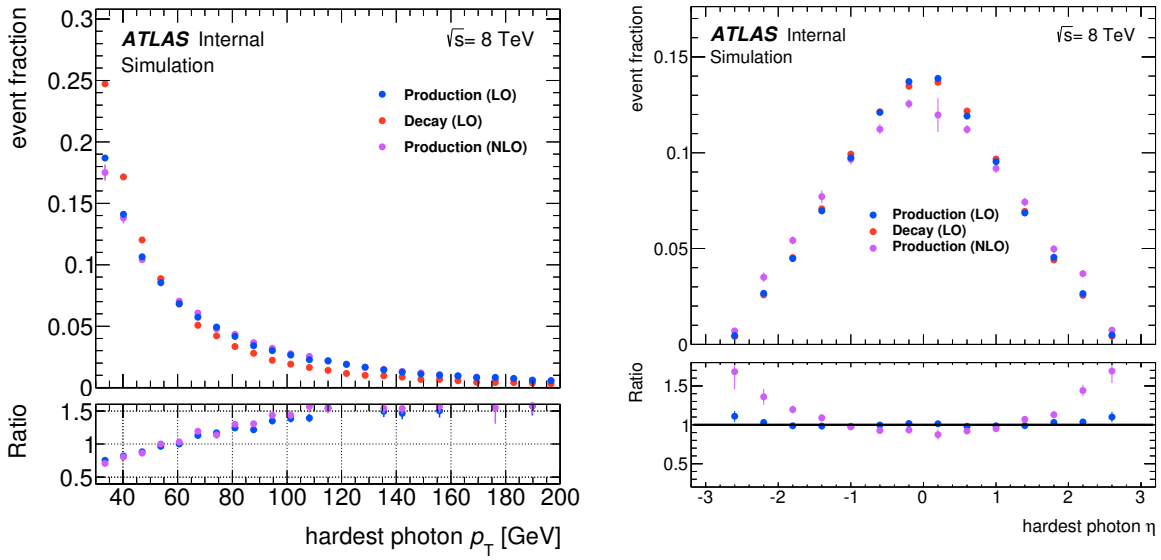

(a) p_T-distribution of the hardest photon.

(b) η-distribution of the hardest photon.

Figure 3.5: Kinematic distributions of the hardest photon.

Figure 3.5 shows the p_T and η distributions of the hardest photon for each event. While the η distribution in Figure 3.5b shows similar shapes for all samples, the p_T-distribution in Figure 3.5a shows a different behavior of the production samples compared to the decay samples for small values of p_T. Both LO and NLO production samples are very similar, which can be seen from the almost constant ratio (purple entries close to the blue entries). In the decay samples the hardest photon has less p_T more often, which is an indication of radiative top decays ($t \to bW\gamma$). This is a first indication that the QED event generator cannot simulate the emissions of photons from top decay products very well, because for LO and NLO the production samples are very similar, while the decay sample is different.

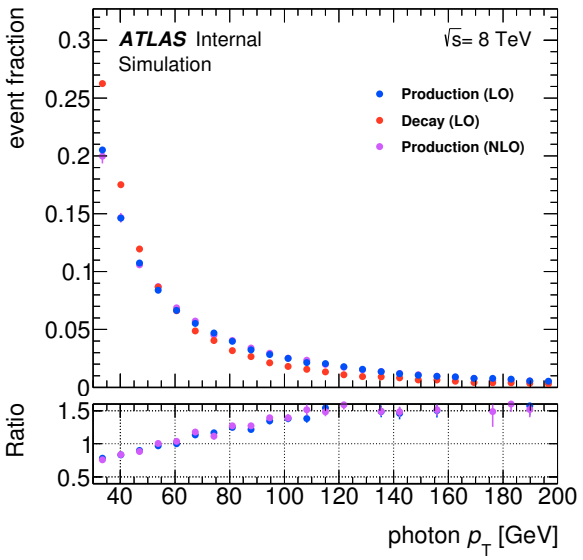

(a) p_T-distribution of all photons.

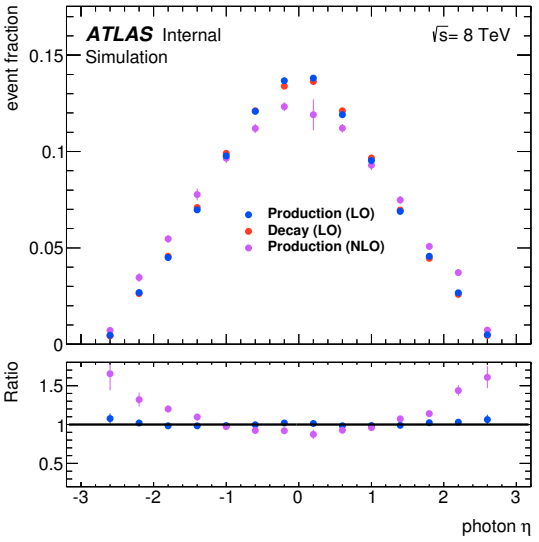

(b) η-distribution of all photons.

Figure 3.6: Kinematic distributions of all photons.

Figure 3.6 shows the p_T and η distributions of all stable photons, passing the object selection. As expected the shapes are very similar to the distributions of the hardest photon.

It is also interesting to look at the influence of the selection to the different samples. This can be seen in the p_T distribution of the top quark.

Figure 3.7 shows the p_T distribution of the hard process top quarks before and after the event selection. Before the event selection, seen in Figure 3.7a, this variable shows the same behavior as previous figures, namely a clear difference of the decay samples compared to the production samples, visible in the peak at $\sim$ 100 GeV. However, after the event selection, seen in Figure 3.7b this excess is not that striking anymore for this specific variable. This can also be seen by comparing the ratio for the two histograms. Before the event selection the ratio increases and after the event selection it fluctuates around 1, for both production samples.

Figure 3.8 shows the ΔR distributions of photons to the leptons, light jets and b-tagged jets, as seen in Figure 3.8a, 3.8b and 3.8c. These figures are done after the object selection but before the isolation cuts are applied. All figures show a typical ΔR shape, with a peak at π. However the decay samples show a different shape for low values of ΔR. This can be seen best in the ΔR distribution of the photons and leptons, because there is only one lepton in each event in comparison to at least 1 b-tagged and at least 2 light jets. The excess at low ΔR values show events with photons very close to a particle, which

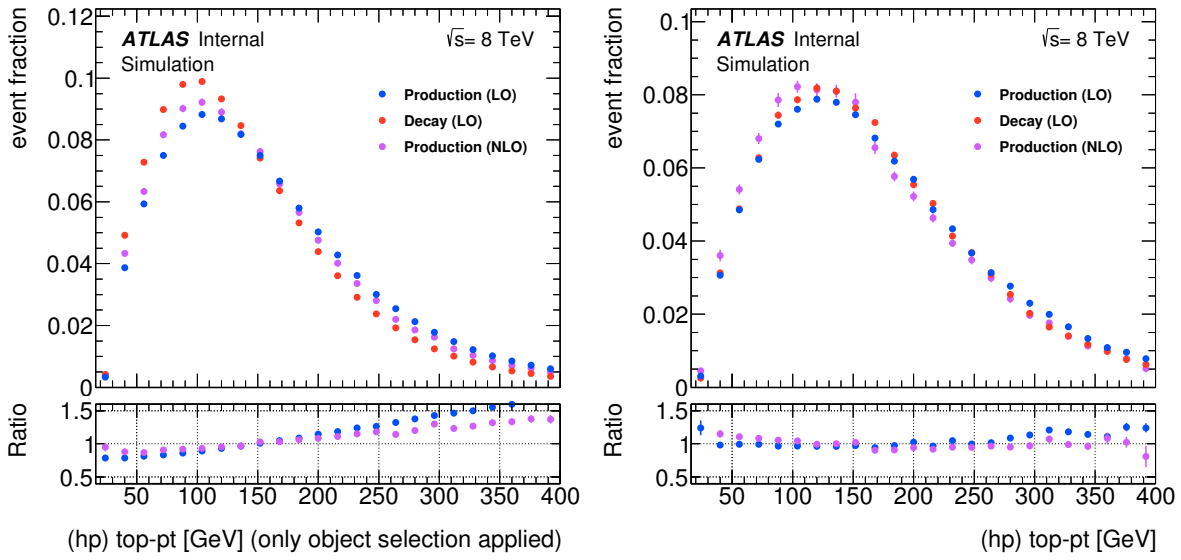

(a) Before the event selection. (b) After the event selection.

Figure 3.7: Comparison of the hard process top p_{T} before and after the event selection.

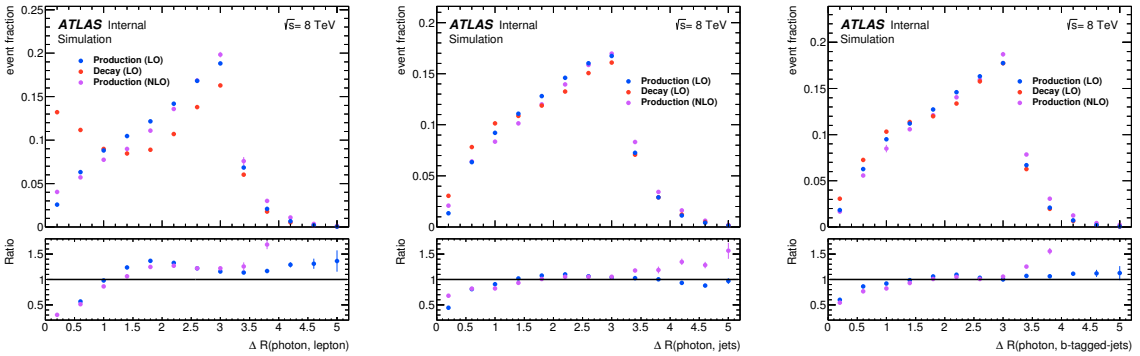

(a) ΔR of photons to leptons. (b) ΔR of photons to light jets. (c) ΔR of photons to b-tagged jets.

Figure 3.8: ΔR distributions of photons to top decay products.

likely radiated the photon. For the ΔR distribution of the photons and both kinds of jets, the differences of the samples drop after $\Delta R = 0.5$, while for the leptons the difference persist until $\Delta R \sim 1$, therefore the isolation cut for the lepton is chosen to be 0.7, while for the jets an isolation cut of 0.5 is sufficient.

In summary the usage of NLO production samples is not preferable, since they fail to simulate the radiative top decays, as seen in the distributions for p_T and ΔR. Therefore the decay sample provides a more accurate description of the $t\bar{t}\gamma$ process including radiative top decays. Unfortunately this comes with the necessity of using large simulation samples, since a large fraction of the events are radiative top decays that will be removed by the event selection.

3.3.2 Influence of QED settings in the event generation

All samples compared so far use the same MC event generator for the QED radiation, namely Photos. In the process of generating the samples, the event generator can be exchanged or even turned off for uncertainty estimates. If different generators for the QED radiation have an impact on the distributions, the decision of preferring the decay samples needs to be revisited, in case the difference of decay to the production samples thins. For this part of the study three different QED generator were used:

- Photos: This is the default generator in terms of QED radiation for this thesis.
- Pythia6: This generator is more often used for the QCD parton showering but can also handle the QED emissions internally, without relying on an external generator like Photos.
- none: QED radiation turned off. This is of course not accurate, but can be used to compare the impact of the QED radiation.

The different QED generators will be tested for the production samples at LO, because they do not allow radiative top decays, which the QED generators have to simulate. Note that the QED emissions from the initial state is simulated by Pythia6, regardless of the chosen QED settings, because the corresponding implementation is more involved and cannot be changed in a straightforward way.

Figure 3.9 shows the number of photons per event before and after the object selection. In Figure 3.9a many photons are present in each event. These photons are very soft and most often come from hadrons. However some differences for the different QED emission settings can be seen. Using Pythia for the QED emission or turning it off makes only a small difference, while for Photos it is more likely to have events with more than 200 soft photons. In Figure 3.9b only a few photons remain after the event selection. Since all $t\bar{t}\gamma$ samples have exactly one photon in the matrix element, the influence of the QED emission can only be seen in events with more than one photon after the object selection, which is a small fraction of the total amount of events.

Figure 3.10 shows the p_T and η distributions of the hardest photon for different QED radiation generators. It can be clearly seen, that the influence of the QED radiation is negligible since all three histograms have almost the same shape and only some small fluctuations can be seen. This is expected, since the hardest photon most often coincides with the photon from the matrix element instead of a photon from the QED emission. Figure 3.11 shows the p_T and η distributions of the second hardest photon for different QED radiation generators. Here, the QED emission is expected to have a larger influence on the p_T distribution of the second hardest photon. Figure 3.12 shows the p_T distribution of the hardest and second hardest light jet for different QED radiation generators. This is just a crosscheck, since the QED radiation is not expected to affect the jet p_T observables. The fluctuations for the jet p_T distributions are roughly as tiny as for the photon p_T distribution, therefore it can be concluded that the

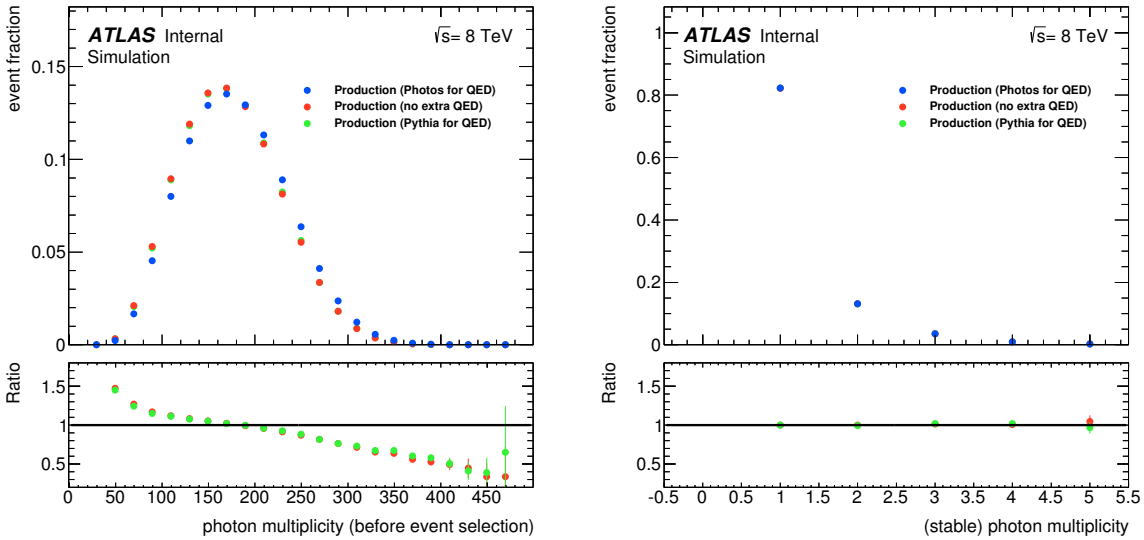

(a) Number of photons before object selection.

(b) Number of photons after object selection.

Figure 3.9: Number of photons before and after the object selection.

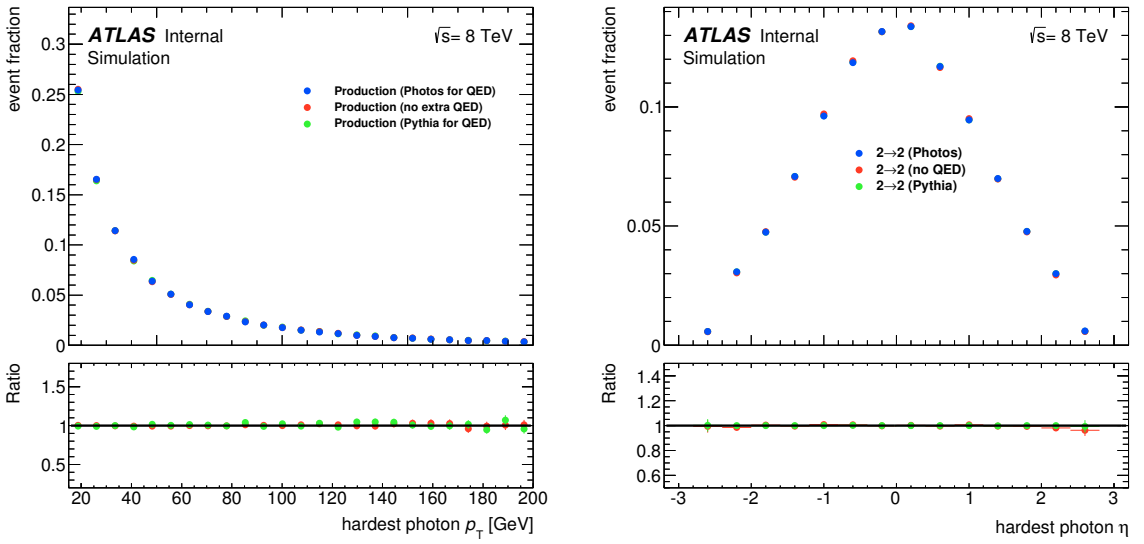

(a) p_{T}-distribution of the hardest photon.

(b) η-distribution of the hardest photon.

Figure 3.10: kinematic distributions of the hardest photon for different QED emission generators.

overall contribution of the QED emission in the samples is rather tiny.
This supports the preference of using the LO decay samples in favor of any of the production samples to simulate the $t\bar{t}\gamma$ process, because the QED emission done by PHOTOS or PYTHIA6 does not significantly affect the production samples.

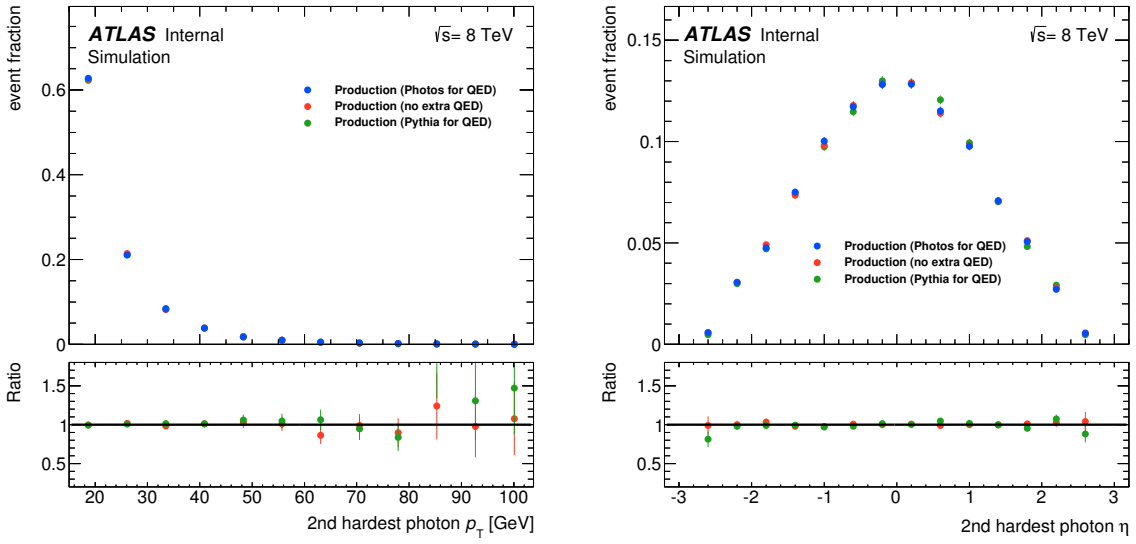

(a) p_{T}-distribution of the second hardest photon.

(b) η-distribution of the second hardest photon.

Figure 3.11: Kinematic distributions of the second hardest photon for different QED emission generators.

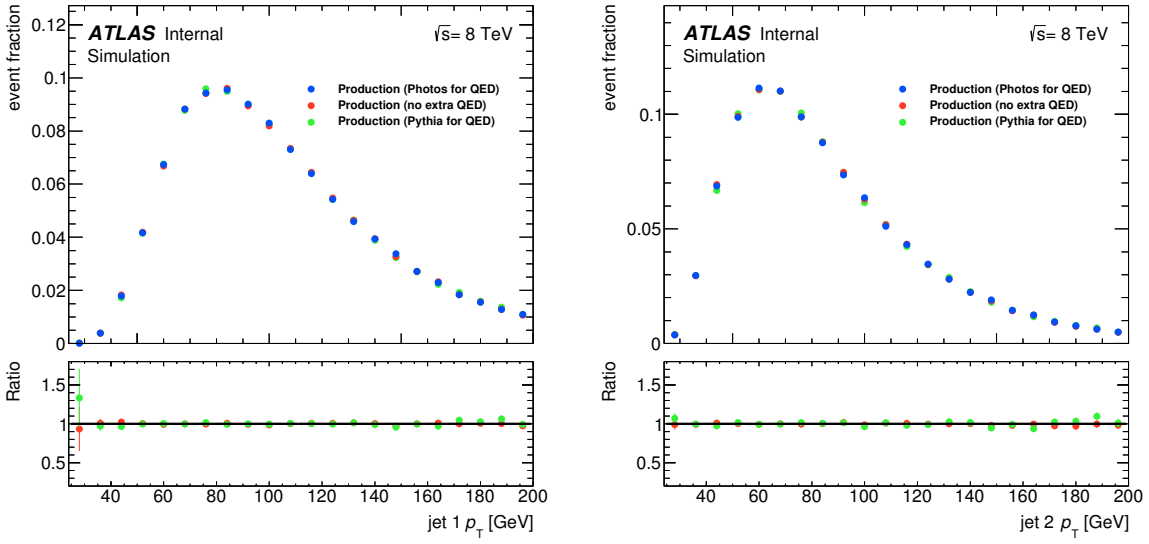

(a) p_{T}-distribution of the hardest jet.

(b) p_{T}-distribution of the second hardest jet.

Figure 3.12: p_{T} distributions of the hardest jets for different QED emission generators.

3.3.3 Reconstruction of the top quarks

In a single lepton $t\bar{t}\gamma$ event, the number of jets expected to come from the hard process partons is four, while there is exactly one lepton. The allocation of the jets to their respective partons is important to be able to reconstruct the hadronically decaying top and hence the leptonically decaying top as well. In addition, multiple jets unrelated to the top quark decay can be found in the events. Therefore an algorithm to relate the jets to the hard process quarks is important. This thesis studies two such algorithms:

- p_{T}^{max}: This method tries to reconstruct the hadronically decaying top quark, by finding the best combination of three jets in terms of their p_{T}. To be more precise, the combination of one b-tagged and two light jets is preferred, since these are the top-quark decay products. For every possible combination, the one with the largest vectorial sum of p_{T} is chosen and attributed to the top decay products. In case only one b-tagged jet is present, a combination of three light jet is also allowed, since the one b-tagged jet could be on the leptonic side of the $t\bar{t}\gamma$ decay.

- KLFitter [37]: This is a fitting tool, which tries to reconstruct a $t\bar{t}$ event by using a kinematic fit. For each possible combination of jets (called permutations) a likelihood function is calculated. The number of possible permutations increases exponentially with the number of jets in an event. Therefore only events with at most eight jets (including b-tagged and light jets) are allowed for KLFitter. Additional constraints, like non physical combinations, e.g. not allowing two b-tagged jets for a single top decay reduce the number of permutations. The permutation with the highest event probability will be chosen by the tool.

Both algorithms try to identify and label the jets, that correspond to the hard process particles. The efficiency of an algorithm is tested by calculating the ΔR value of the hard process particle to the labeled jet, e.g. the ΔR of the leptonic b-quark to the leptonic b-jet. For a match of the parton and the jet, the ΔR value has to be lower than 0.3 [37]. Additionally each considered event has to be truth-matched, as explained below.

Truth matching

Truth matching is an important procedure to test the agreement of the hard process event simulation and the parton showering. To test if an event is truth matched, the partons of the hard process are compared to all jets in the event. For a single lepton $t\bar{t}$ or $t\bar{t}\gamma$ event, the available partons are two b-quarks (one from each top decay) and two light quarks (from the hadronic W decay). For each parton at least one jet has to be found in a ΔR-distance of 0.3 (similar to the jet reconstruction, which uses 0.4). An additional constraint is to require only light jets for the light quark partons and only b-tagged jets for the b-quark partons. In case of missing b-tagged jets, due to the limited b-tagging efficiency of 70%, light jets are also allowed for the b-quark partons, but not vice versa (since the mistag is small and it is neglected in this study). If every parton matches to a jet, the event is considered to be truth matched.

Sample	Truth-matching efficiency
production (LO)	0.423
production (NLO)	0.418
decay (LO)	0.343

Table 3.4: Truth matching efficiencies.

Table 3.4 shows the truth matching efficiencies for the discussed samples. The statistical uncertainties on the efficiencies is less than 10^{-3}, since all samples have a large number of events. The event selection is applied before an event is asked to be truth matched. Since truth matching is a quantity that can only be calculated using samples with a truth record, it is required only for calculating the reconstruction efficiencies of the algorithms, but not for the figures in this Section.

Evaluation of the algorithms

Once the truth matching is passed successfully, an event has jets close to all partons. That doesn't necessarily mean that the jets match their corresponding partons if the event has more than four jets. Without a reconstruction algorithm, it is not possible to tell which parton belongs to which jet. There are basically two quantities that can be tested for both algorithms:

- the reconstruction efficiency,
- the difference between the samples.

The first item was discussed already and is the obvious number to compare. However the second item is also important, since an additional difference between the production and the decay samples can further enhance the sensitivity to the $t\bar{t}\gamma$ coupling.

Reconstruction efficiency

For the reconstruction efficiencies, the numbers can be calculated easily. Additionally the requirement on the number of jets can be changed a little, to see the impact on the reconstruction efficiencies.

Table 3.5 shows the reconstruction efficiencies for both algorithms with different amount of reconstructed jets required per event. The first configuration comes with the highest efficiencies, which is expected, but also neglects the largest fraction of events. The second configuration is the more realistic one, since in a real measurement the b-tagging efficiency often leads to misidentify b-jets as light ones.

Jet configuration	Sample	p_{T}^{max} efficiency	KLFitter efficiency
= 2 b-jets & 2 light-jets	production (LO)	0.530	0.944
	production (NLO)	0.522	0.928
	decay (LO)	0.455	0.906
≥ 1 b-jet, ≥ 3 light jets	production (LO)	0.419	0.704
	production (NLO)	0.400	0.686
	decay (LO)	0.356	0.649

Table 3.5: Reconstruction efficiencies of the algorithms for different jet configurations.

Regardless of the chosen jet configuration, the KLFitter method clearly performs better in pairing the jets in a correct way. Both methods can handle the production samples better than the decay samples, which can be explained as due to photons radiated from jets in the decay samples. Those decays can modify the kinematics of the jets and make the reconstruction more difficult.

Difference of the samples

For the second item, that needs to be tested, a look at invariant mass distributions is useful. They can be calculated by adding the four-vectors of the reconstructed jets, which are often the decay particles. However the two methods are not completely comparable for their invariant mass distributions. While the KLFitter tool does not take the kinematics of the photon into account, the p_{T}^{max} algorithm can be extended to contain the four-vector of the photon for the invariant mass distribution. KLFitter forces the invariant mass of a given particle to match their physical mass. On the other hand, the p_{T}^{max} method does not know beforehand, where the photons are radiated from. Before looking at the invariant mass distribution of the top quark, the invariant mass of the W boson shows some features, which are interesting for the p_{T}^{max} method.

Figure 3.13 shows the invariant mass of the hadronically decaying W boson reconstructed using the p_{T}^{max} method. While Figure 3.13a shows the invariant mass of the two light jets with an additional photon, Figure 3.13b shows the invariant mass of only the two light jets. This means that Figure 3.13a is the correct one, for events in which the photon is radiated from the W boson or its decay products, while Figure 3.13b is the correct one for events where the photon is radiated from somewhere else. Figure 3.13b shows the invariant mass of the W boson only. Most of the times the photon will be radiated from somewhere else (which explains the sharp peak), but if the invariant mass of a top quark itself is considered, this balance will shift to a lower rate (of the photon being radiated from the initial state, the other top or its decay products) in a $t\bar{t}\gamma$ event. For the purpose of reconstruction this is unfortunate, but for the purpose of differentiating the production samples from the decay samples, the invariant mass distributions with an additional photon can offer a good discrimination, because photons cannot be radiated from the top decay products in the production samples.

Figure 3.14 shows the invariant mass of the leptonically decaying W boson reconstructed using the p_{T}^{max} method. The difference in the two figures is again the addition (or not) of the photon for the invariant mass. Since in the single lepton channel the reconstruction of the leptonically decaying W is easier, the difference of the production and the decays samples is even more obvious in Figure 3.14.

For the KLFitter tool, an invariant mass distribution of any of the W bosons is not sensible, since the fit fixes the mass of the W bosons to the physical value. However the top quark mass can be added as a free parameter to the fit.

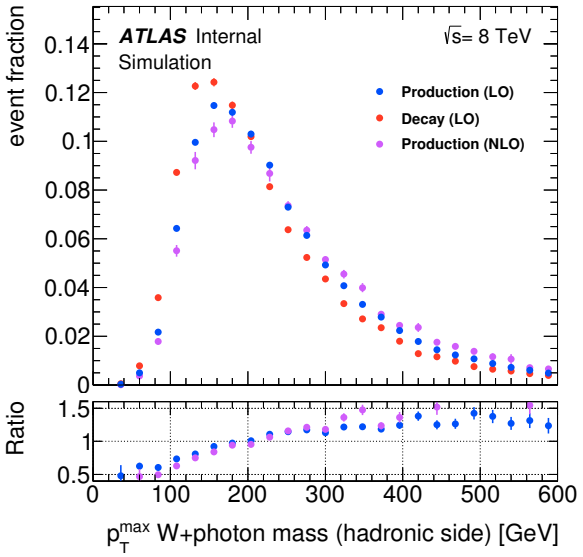

(a) Invariant mass of two light jets + a photon.

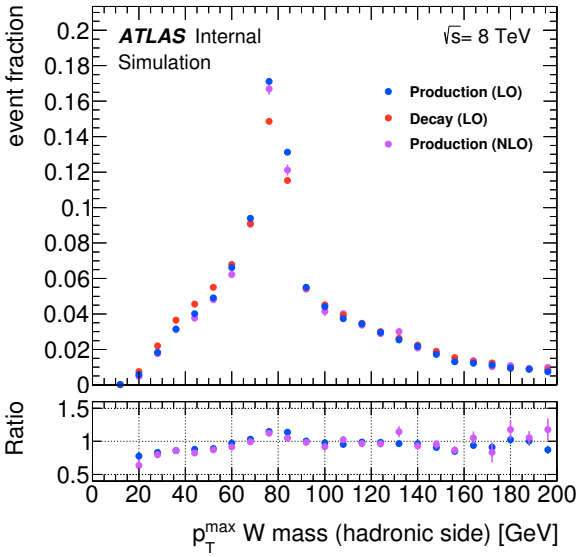

(b) Invariant mass of two light jets.

Figure 3.13: Invariant mass distributions of the hadronically decaying W boson with the p_{T}^{max} method.

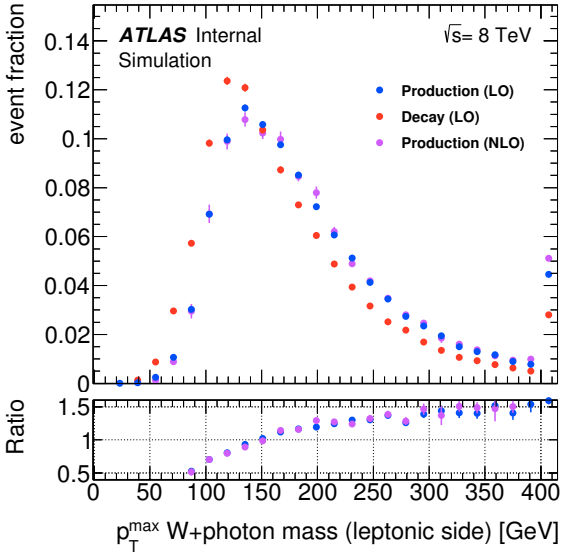

(a) Invariant mass of the lepton and $E_{\mathrm{T}}^{\mathrm{miss}}$ + a photon.

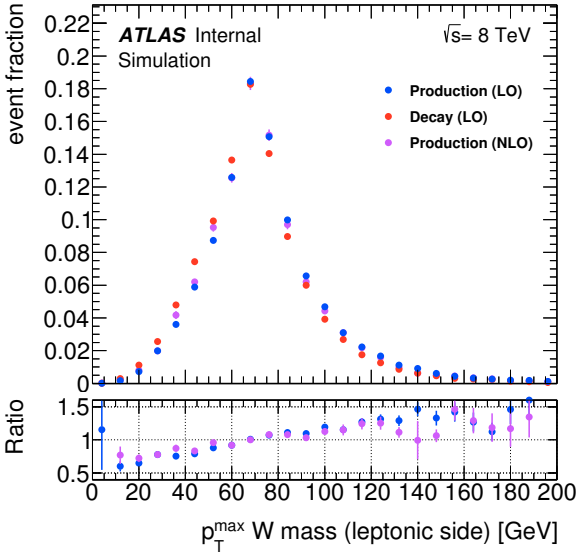

(b) Invariant mass of the lepton and $E_{\mathrm{T}}^{\mathrm{miss}}$.

Figure 3.14: Invariant mass distributions of the leptonically decaying W with the p_{T}^{max} method.

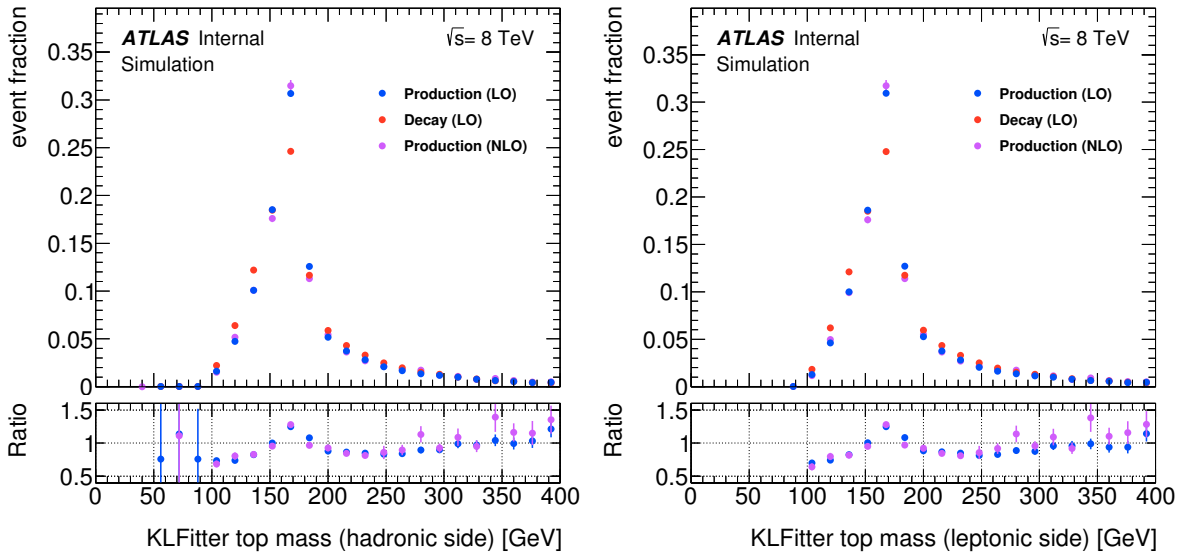

(a) Hadronically decaying top quark.

(b) Leptonically decaying top quark.

Figure 3.15: Invariant mass distributions of the top quarks, using the KLFitter tool.

Figure 3.15 shows the invariant mass distributions of both top quarks, using the KLFitter tool. While both distributions clearly peak around the top quark mass, a distinction between the samples is impossible, because the fitting tool forces this behavior. When using KLFitter, it is allowed to have a fixed top mass or use it as a free parameter for the fit. For this study a free top quark mass with the initial value of 172.5 GeV was used [37], which means although the top quark mass is a free parameter, the initial value of the fit will have a peak around 172.5 GeV in the invariant mass distribution. However the widths of these distributions show, that the reconstruction of the top quarks works rather well with the KLFitter tool.

Figure 3.16 shows the invariant mass distributions of the leptonically decaying top quark, using the p_{T}^{max} method. Again the left histogram includes the kinematics of the photon, while the other one does not. Neither of the distributions peak around the top quark mass, because the events, where the kinematics of the photon are missing or mistakenly added. Still in Figure 3.16a a difference of the decay and production samples can be seen, but not as clear as in the W boson mass distributions.

Figure 3.17 shows the invariant mass distributions of the hadronically decaying top quark, using the p_{T}^{max} method. These invariant mass distributions show the same behavior as the ones for the leptonically decaying top quark and only the shapes differ a bit.

In conclusion, the KLFitter algorithm provides a good reconstruction of the top quark, while the p_{T}^{max} method performs worse in terms of reconstruction, because of the unknown origin of the photon. On the other hand, in terms of differentiating production and decay samples, the invariant mass figures of the p_{T}^{max} method show some shifts in the peak positions (especially for the W boson mass distribution seen in Figures 3.14 and 3.13). The KLFitter algorithm does not allow to use the W boson mass as a free parameter and fixes the peak position for the top quark mass. Therefore the usage of the p_{T}^{max} method is preferred in terms of differentiating the production and decay samples, while the KLFitter algorithm provides the better reconstruction of the top quark. It is important that the KLFitter framework currently does not support the presence of extra photons. Therefore the advantage of using KLFitter is limited for our purpose and the p_{T}^{max} algorithm is preferred for this study.

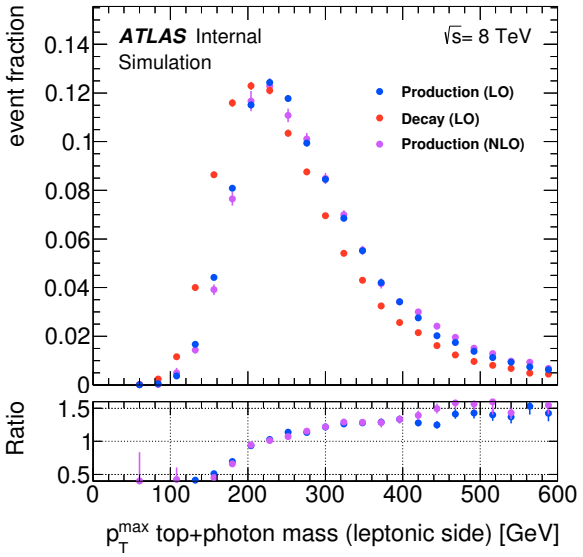

(a) Leptonically decaying top quark + a photon.

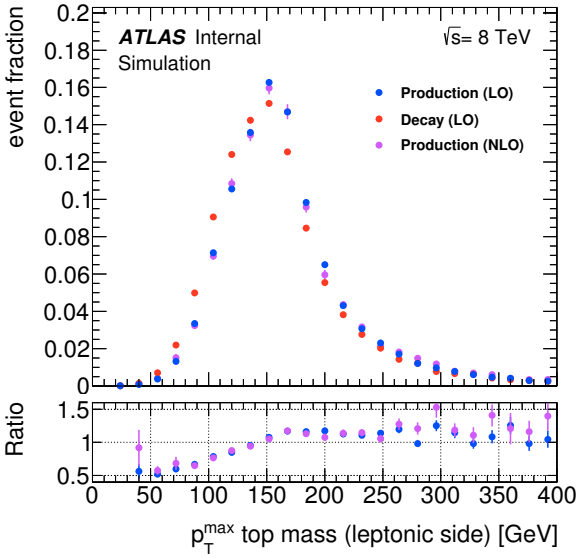

(b) Leptonically decaying top quark.

Figure 3.16: Invariant mass distributions of the leptonically decaying top with the p_{T}^{max} method.

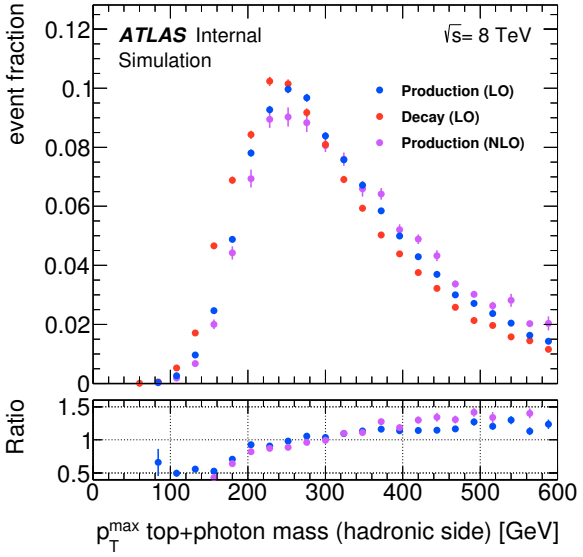

(a) Hadronically decaying top quark + a photon.

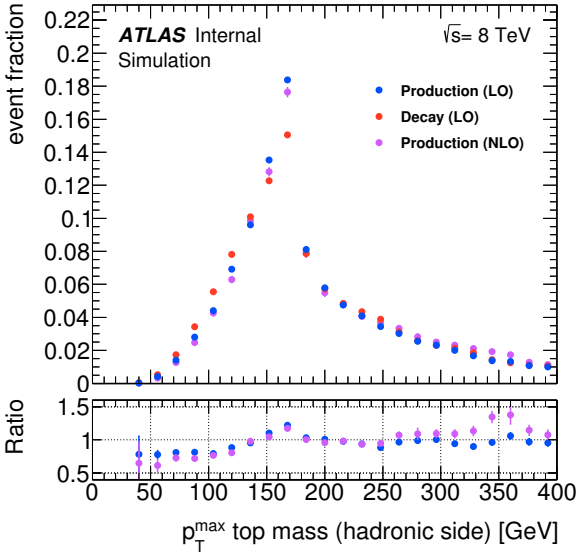

(b) Hadronically decaying top quark.

Figure 3.17: Invariant mass distributions of the hadronically decaying top with the p_{T}^{max} method.

3.3.4 Influence of QCD generators

Apart from changing the QED settings in the event generation it is important to study how different event generators handle the QCD parton shower in the event generation, because of possible effects on the event selection. The default generator for the parton shower used for this thesis is PYTHIA6. The impact on the distributions using different parton shower generators will be used as an estimation for the systematic uncertainties, when using PYTHIA6 as default generator for the parton shower. In this Section, three different parton shower generators will be compared, using the $t\bar{t}\gamma$ decay samples at LO:

- PYTHIA6: This is the default generator for the parton shower for this thesis.
- FORTRAN HERWIG: This generator is used for many physics analyses [29] and was also used in the 7 TeV $t\bar{t}\gamma$ analysis [22] in combination with MADGRAPH for the hard process and PHOTOS for the QED radiation. Using this generator for the parton shower will reproduce this configuration and make the 8 TeV analysis comparable.
- HERWIG++: This is an improved version of the generator HERWIG [30]. This generator has the disadvantage of handling the QED emission on its own, not allowing to transfer it to PHOTOS. However judging from the small impact of the QED emissions on the distributions in Section 3.3.2, this effect should be negligible.

Each of these three generators has a different kind of truth record. While PYTHIA6 assigns all hard process particle their own status code, making them easily accessible, the other two generators have a different implementation, explained in Appendix A.1.2. This makes the calculation of truth matching and reconstruction efficiency impossible, since the ΔR of the parton and the corresponding jets cannot be calculated. However the kinematic distributions of the photon, or the top quark mass distributions only need the information of the stable particles, which are accessible for all parton shower generators.

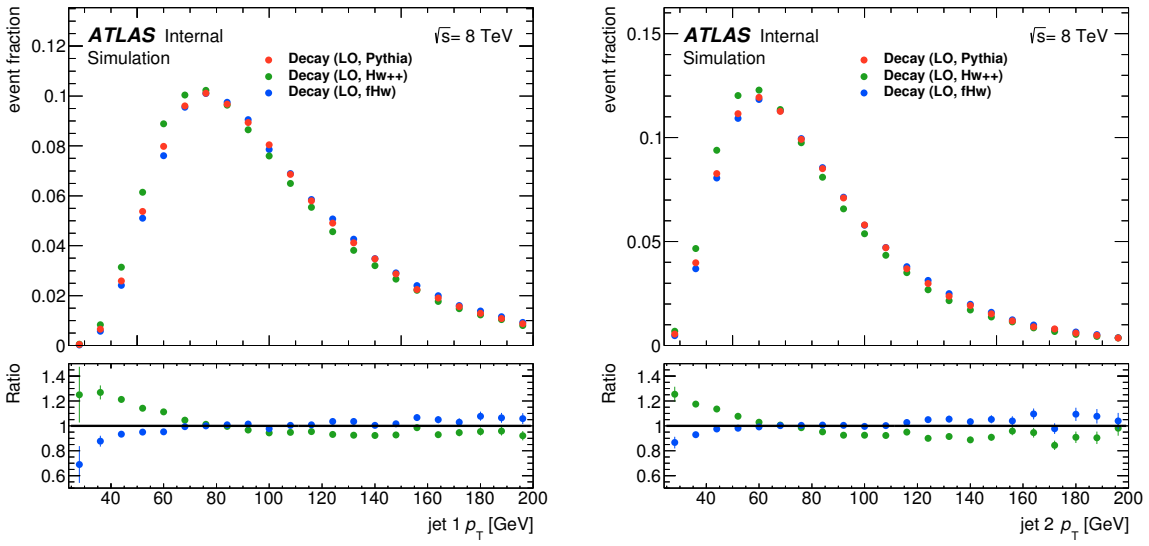

(a) p_T-distribution of the hardest jet.

(b) p_T-distribution of the second hardest jet.

Figure 3.18: p_T distributions of the hardest jets for different parton shower generators.

Figure 3.18 shows the p_T distributions of the hardest jets in each event, for different parton shower generators, with the hardest jet in Figure 3.18a and the second hardest jet in Figure 3.18b. For both figures FORTRAN HERWIG and PYTHIA6 show very little differences, while HERWIG++ has some excess for low values of p_T. Therefore the parton showering in HERWIG++ behaves differently to PYTHIA6 and FORTRAN HERWIG, which will reflect in additional systematic uncertainties for the $t\bar{t}\gamma$ analysis. Additional jet p_T distributions can be found in Appendix A.2. Since there is a small difference for the HERWIG++ parton shower generator, some photon related quantities have to be checked, because HERWIG++ generates the QED emission by itself.

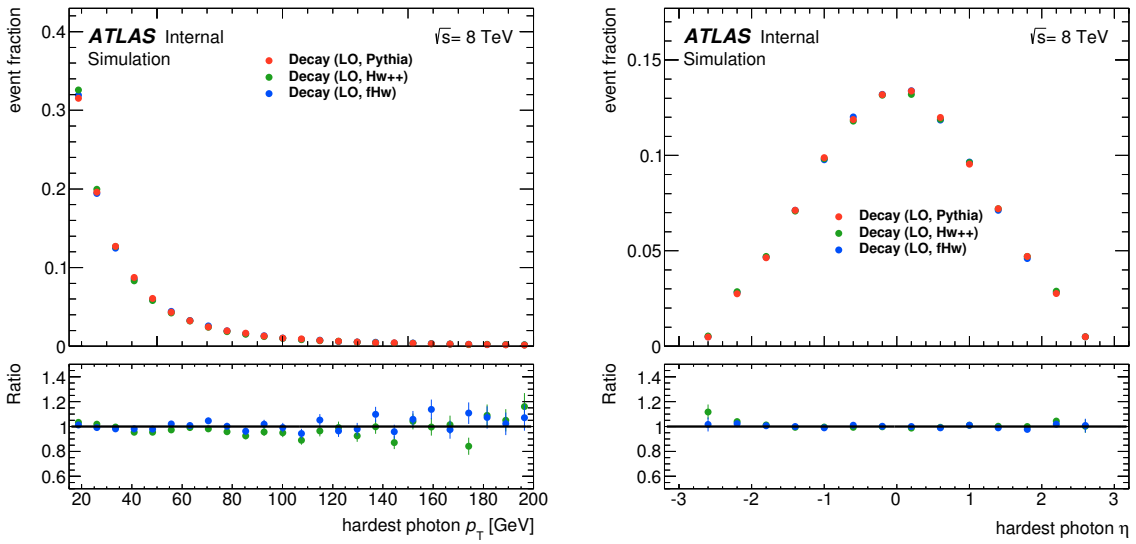

(a) p_T-distribution of the hardest photon.

(b) η-distribution of the hardest photon.

Figure 3.19: Kinematic distributions of the hardest photon for different parton shower generators.

Figure 3.19 shows the p_T and η distribution of the hardest photon in each event, for different parton shower generators. As indicated in the p_T distributions of jets, the differences between PYTHIA6 and FORTRAN HERWIG are negligible here as well. Since the shape of the HERWIG++ distributions also shows almost no differences to the other two generators, an influence of the QED emission can be ruled out.

Figure 3.20 shows the p_T and η distribution of the second hardest photon in each event, for different parton shower generators. Photons radiated from hadrons due to the parton shower are expected to have less p_T than the photon from the hard process. Therefore the photons in Figure 3.20 are more likely to come from the parton shower than the photons in Figure 3.19. However also for the second hardest photon, the influence of other parton shower generators is small.

Figure 3.21 shows the number of photons (after the event selection is applied) for different parton shower generators. As expected (see Figure 3.4) most events have only one photon, even for other parton shower generators. Since the requirement on the photon's p_T is lowered to 15 GeV for the comparison of different parton shower generators, there are more events with more than one photon, but this fraction is small.

Table 3.6 shows the number of photons (after the event selection is applied) for different parton shower generators. The fractions correspond to Figure 3.21. In conclusion the different parton shower generators do not behave differently enough to redo the comparison of LO and NLO with another parton

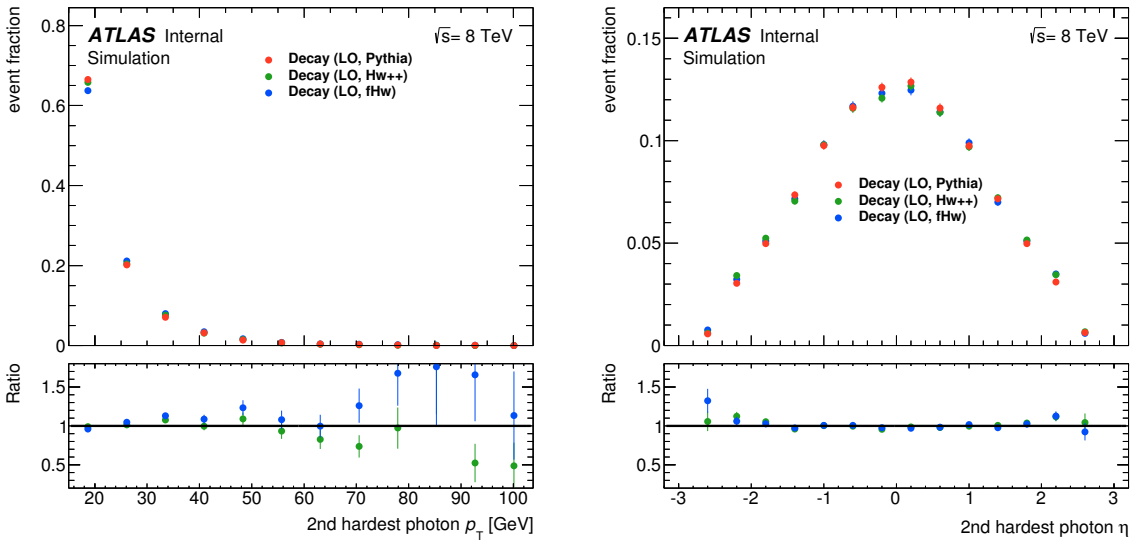

(a) p_T-distribution of the second hardest photon. (b) η-distribution of the second hardest photon.

Figure 3.20: Kinematic distributions of the second hardest photon for different parton shower generators.

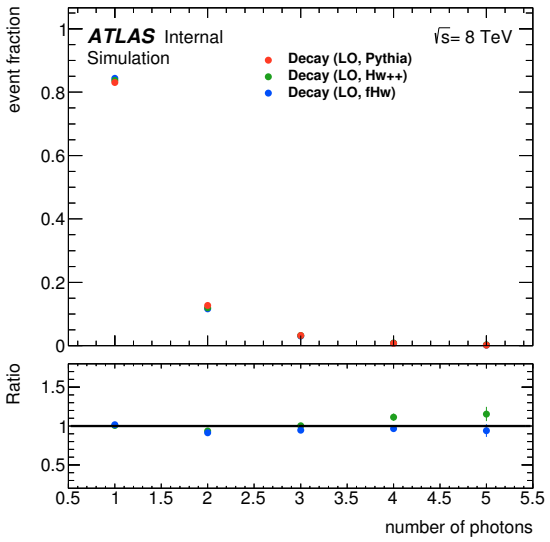

Figure 3.21: Number of photons for different parton shower generators.

Photon multiplicity	PYTHIA6	FORTRAN HERWIG	HERWIG++
Exactly one [%]	83.1	84.4	83.7
More than one [%]	16.9	15.6	16.3

Table 3.6: Event fractions for the number of photons for different parton shower generators.

shower generator.

CHAPTER 4

Measurement of the $t\bar{t}\gamma$ cross section in the dilepton channel

4.1 Motivation

This chapter describes a complete $t\bar{t}\gamma$ analysis performed in the dilepton channel, using 8 TeV data collected by the ATLAS detector at the LHC, with the goal to measure the total $t\bar{t}\gamma$ cross section. The number of events in the dilepton channel is significantly lower than in the single lepton channel, because of the branching ratio of $W \to \ell\nu$. This analysis focuses on the eμ-channel specifically, because of the excellent signal-to-background ratio. The ee- and $\mu\mu$-channels have large contributions from backgrounds involving the Z boson. In case of a $W \to \tau\nu_\tau$ decay, the decay of the τ lepton is taken into consideration, because it is able to decay into an electron or a muon. Therefore the leptonic decays of the τ-lepton are included for the ee $\mu\mu$ and $e\mu$ channels.

So far no $t\bar{t}\gamma$ cross section measurement in the dilepton channel has been published for any of the experiments. The $t\bar{t}\gamma$ cross section measurements published by the ATLAS experiment at 7 TeV [22] and the preliminary result released by the CMS experiment at 8 TeV [23] were performed in the single lepton channel. In the dilepton channel, the statistical uncertainty is expected to play a more important role due to its smaller branching ratio. In the existing measurements the systematic uncertainty was larger than the statistical uncertainty. Some of the systematic uncertainties are expected to be smaller in the dilepton than in the single lepton channel. For example uncertainties due to jet modeling, which was the dominant systematic uncertainty in Reference [22], are expected to be significantly smaller in the dilepton channel, because of the lower number of jets in this channel. In this thesis, an optimal event selection that minimizes the total (statistical and systematic) expected uncertainty on the measured cross section, is studied. Despite the larger expected statistical uncertainty, the measurement might reach precision comparable to the measurement in the single lepton channel, in case the systematic uncertainty is significantly lower. Both the measurements in the single lepton and the dilepton channel are complementary, because they are affected by different background processes.

4.2 Description of the data and simulation samples

The samples used for the analysis consist of data samples measured with the ATLAS detector and MC samples for the signal process as well as multiple MC samples for different background processes, which aim to model the data. The information on how the samples were normalized relies on Reference [38].

4.2.1 Data and signal MC samples

- Data:
  The data used in this analysis was taken at a centre-of-mass energy of 8 TeV with an integrated luminosity of 20.3 fb^{-1}. Each event has to pass one of the single-lepton triggers and includes on average 20 pileup events. Pileup describes additional proton-proton interactions besides the main interaction.

- Signal:
  The simulated signal sample used for the $t\bar{t}\gamma$ process is the same as the one used in Section 3 in the generator studies. However for this analysis full detector simulation [39] was added, to be able to compare measured data with simulation and to calculate modeling of objects for the systematic uncertainties.

4.2.2 The SM background processes

Since this analysis focuses on the different lepton-flavour (eμ) channel only, the background contribution is small. In the same lepton-flavour channel, a large amount of background processes involve the Z boson, which can decay into two leptons of the same flavor and is therefore easily misidentified as the $t\bar{t}$ dilepton channel in data. To be more specific, the Z with additional jets background process is much more abundant than the $t\bar{t}\gamma$ process and would appear as a large background in the same lepton-flavour channel.

The largest fraction of background events in the different lepton-flavour channel contain photons radiated from hadrons in SM processes which are either $t\bar{t}$ dilepton events or processes with similar decay products. Therefore only backgrounds with two real leptons are considered in this study:

- Photons from hadrons:
  This category includes background processes where photons are produced in hadron decays. The photons from hadron decays are identified using the event generator information.

  - $t\bar{t}$:
    Prior to selecting a photon (see Section 4.3.2), this process dominates other backgrounds and is even larger than the signal, since the only difference to the signal process is an additional photon. The $t\bar{t}$ sample was normalized to the NNLO+NNLL cross section predictions. The contribution from photons not radiated from hadrons in the $t\bar{t}$ samples is described by the signal $t\bar{t}\gamma$ sample and removed from the $t\bar{t}$ MC sample, using truth information. This process is generated with POWHEG and PYTHIA6.
  - Z with additional jets:
    The contribution from photons, e.g. radiated by the leptons from the decay of the Z boson, is described by the $Z\gamma$ sample. This process is generated with SHERPA

- $W\gamma$ and $Z\gamma$:
  These processes are generated with SHERPA. The normalization corresponds to the cross section predicted by SHERPA. Both, for these samples and the Z with additional jets sample the Z cross sections were set to the NNLO predictions.

- Single top in the Wt channel:
  Since for the different single top processes only the Wt channel results in two W bosons, which can further decay to two leptons in total, the other single-top processes are not considered as

relevant backgrounds. The sample was normalized to approximate NNLO cross section. The contribution of the photons radiated from hadrons in this channel is neglected for this analysis, due to the small contribution. The process is generated with POWHEG and PYTHIA6.

- Diboson:
  This process is generated with ALPGEN and HERWIG. The sample was normalized to the NLO QCD cross section predictions.

4.3 Object and event selection

This study in the dilepton $t\bar{t}\gamma$ channel uses data from the ATLAS detector and MC signal and background events as described in the previous section. The event selection is optimized such that the combined statistical and systematic uncertainty on the cross section measurement is minimized. An optimization of certain requirements will be part of the analysis, which will not be mentioned in this Section, but covered in Section 4.4.1. For the remaining requirements in the event selection, the values were chosen to be identical as in the study of the single lepton channel in Section 3.2 and in Reference [38].

4.3.1 Object selection

This part of the selection describes how the physics objects are selected, but does not introduce any requirements to an event.

- Leptons are required to have a p_{T} of at least 25 GeV. At least one of the leptons must be matched to the lepton that triggered the event. The charges of the two leptons have to be opposite.

- Photons are required to have at least a certain amount of transverse momentum (the exact value will be determined in the optimization). In the simulated samples, the photons are classified according to their origin as either photons from hadrons or signal photons. Photons from electrons are not taken into consideration, since the rate of misidentified photons, which are actually electrons is small in the dilepton channel. To ensure to have a photon not radiated from a hadron, the photons' parent has to have a PDG-ID of at most 24 (see Section 3.1). This classification is used to avoid double-counting of signal and background events. If a $t\bar{t}$ or a Z boson with additional jets sample, without photons in the hard process, is used to estimate the background due to photons from hadrons, the photons are required to be classified as photons from hadron origin, accordingly. On the other hand, when $t\bar{t}\gamma$ or $Z\gamma$ with jets samples with photons in the hard process are used to estimate the yields of events with prompt photons, the photons are required to be classified as signal photons.

- Jets are reconstructed with the anti-k_{t} algorithm [40] with radius parameter of R=0.4. They are required to have at least 25 GeV of p_{T}. Since this study uses data, a simulation of the b-tagging efficiency with a random number generator, as used in Section 3.2, is not needed. Instead, the jets are tagged as likely to have originated from b-quarks using the MV1 algorithm [41] with a tagging efficiency of about 70%. The mistag rate (light jets recognized as b-tagged jets) is neglected for this analysis, since it is a small fraction [36].

For all leptons, photons and jets, in addition to the listed requirements, the absolute value of η should be in the range of 0 to 2.5.

4.3.2 Event selection

This part of the selection describes the requirements for an event in order to be kept for further consideration.

- The number of leptons should be exactly two (one electron and one muon), to ensure having a dilepton event instead of having fully hadronic, single lepton or background events.
- The number of photons should be exactly one.
- The number of jets (light and b-tagged jets) should be at least one. Additionally, since a $t\bar{t}\gamma$ event in the dilepton channel is expected to feature at least two b-jets, at least one of the jets (if there are more than one in the event) has to be b-tagged.

p_{T}-cone20 and E_{T}-cone40

In this analysis the isolation requirements are made of ΔR requirements, which are used similarly to the ones in the generator study in Section 3 as well as the variables p_{T}-cone20 and E_{T}-cone40.

- p_{T}-cone20: This variable is defined as the scalar sum of p_{T} for all charged tracks in a ΔR cone of 0.2 around a photon in the event [42].
- E_{T}-cone40: This variable is defined as the sum of E_{T} in the calorimeter cells from both the electromagnetic and hadronic calorimeters in a ΔR cone of 0.4 around a photon in the event, excluding cells corresponding to the photon candidate [42]. In this context E_{T} is obtained from the energy, measured in the calorimeters, projected on the transverse plane (by obtaining the angle of the track, that corresponds to the entry in the calorimeter).

Both the ΔR requirements as well as the requirements on p_{T}-cone20 and E_{T}-cone40, are part of the optimization, described in Section 4.4.1. Since p_{T}-cone20 and E_{T}-cone40 are part of the isolation requirements, they are also capable of distinguishing isolated particles from particles near other objects. Both p_{T}-cone20 and E_{T}-cone40 are used to separate isolated photons from photons stemming from hadron decays. They are very efficient tools to suppress photons radiated in jets. However photons radiated from e.g. leptons have to be suppressed by using the corresponding ΔR requirement.

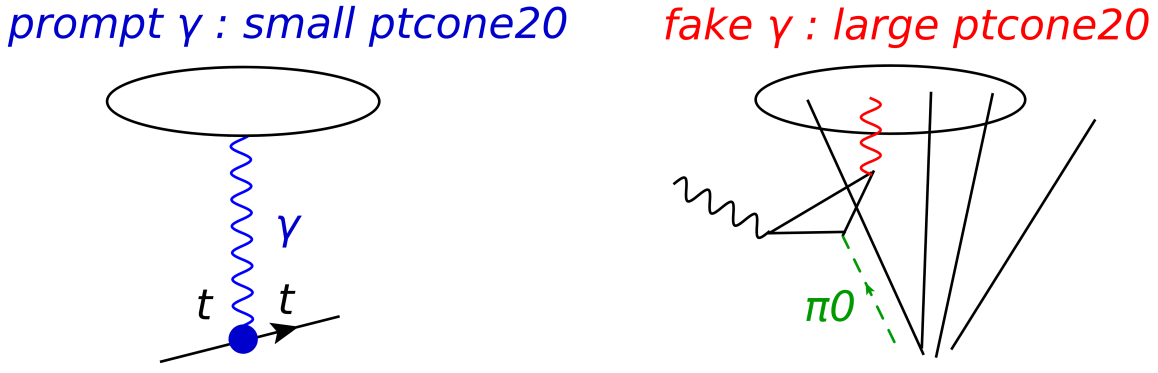

(a) An isolated photon candidate.

(b) A photon produced by a π_0 decay inside a jet.

Figure 4.1: Illustration of the p_{T}-cone20 variable.

Figure 4.1 illustrates how the p_{T}-cone20 variable is able to distinguish photons radiated from isolated objects (like a top quark) from photons radiated close to a jet.

4.3.3 Kinematic distributions

Before performing the optimization of the event selection a good data and MC agreement has to be ensured.

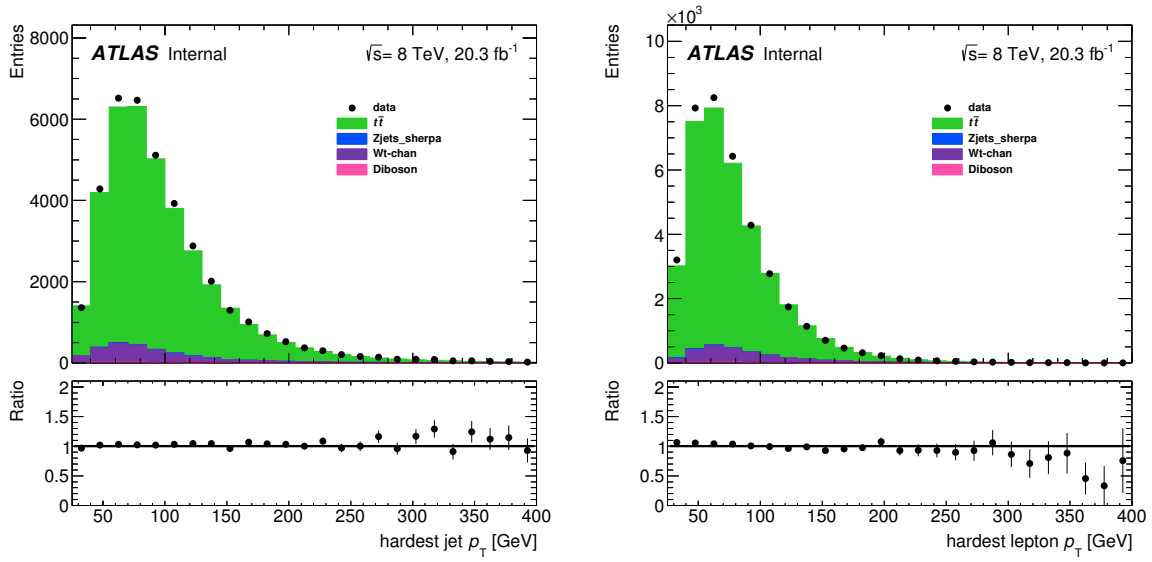

(a) Hardest jet p_{T}.

(b) Hardest lepton p_{T}.

Figure 4.2: p_{T} distributions of the hardest jet and lepton for data compared to simulation.

Figure 4.2 shows the p_{T} distributions of the hardest jet (a) and the hardest lepton (b). In this Figure (and the corresponding figures in Section 4.5.1) data events, shown as black dots, are compared to the theory prediction obtained from the MC generator samples. Only statistical uncertainties are shown. The histograms in Figure 4.2 are filled before requiring one photon in each event. Therefore both distributions are dominated by the $t\bar{t}$ background. The single top production in the Wt channel (labeled as Wt-chan) is the second largest source of background. The contribution of other background processes are small. For consistency it is important to check the data and MC agreement before and after the event selection. Figure 4.2a shows that these two distributions are well described by the data.

4.4 Analysis strategy

The goal of this analysis is to measure the $t\bar{t}\gamma$ cross section at 8 TeV. Due to the excellent signal-to-background ratio in the $e\mu$ channel a cut-and-count analysis strategy is chosen. The results are obtained through an optimization of the event selection.

4.4.1 Optimization of the event selection

The goal of the optimization of the event selection is to find a particular set of requirements, which have the lowest expected relative uncertainty on the cross section measurement.

Expected cross section

The expected cross section $\hat{\sigma}$ and its uncertainty $\Delta\hat{\sigma}$ can be calculated using the MC samples for signal and background.

$$\hat{\sigma} = \frac{N_{data}^{expected} - N_{background}}{\epsilon \cdot \mathcal{L}} = \frac{(N_{signal} + N_{background}) - N_{background}}{\epsilon \cdot \mathcal{L}} = \frac{N_{signal}}{\epsilon \cdot \mathcal{L}} \tag{4.1}$$

Equation 4.1 shows the definition of the expected cross section $\hat{\sigma}$, containing the Luminosity $\mathcal{L}$, the efficiency ϵ and the expected number of events in data $N_{data}^{expected}$. The expected cross section does not use events from data, $N_{data}^{expected}$ is calculated using the events of the signal and background samples N_{signal} and $N_{background}$ only, the Luminosity $\mathcal{L}$ and the efficiency ϵ.

Although the expected cross section $\hat{\sigma}$ is independent of the number of background events $N_{background}$, as it cancels out in the equation, it is shown in the equation to highlight the contribution of $N_{background}$ to the statistical uncertainty. The efficiency ϵ represents the efficiency of the object and event selection.

$$\epsilon = \frac{N_{signal}}{N_{signal}^{initial}} \tag{4.2}$$

Equation 4.2 shows the definition of the efficiency ϵ. It consists of the amount of events in the signal sample after the full selection N_{signal} and the amount of events initially in the MC signal sample $N_{signal}^{initial}$.

It is useful to separate the uncertainty of the expected cross section $\Delta\hat{\sigma}$ into a statistical and a systematic uncertainty.

$$\Delta\hat{\sigma} = \sqrt{(\Delta\hat{\sigma}_{stat})^2 + \left(\Delta\hat{\sigma}_{syst}\right)^2}\,. \tag{4.3}$$

Using error propagation, the uncertainties can be computed as:

$$\begin{aligned} \Delta\hat{\sigma}_{stat} &= \sqrt{\left(\frac{\Delta\left(N_{signal} + N_{background}\right)}{\epsilon \cdot \mathcal{L}}\right)^2 + \left(\frac{\Delta N_{background}}{\epsilon \cdot \mathcal{L}}\right)^2} \\ &= \sqrt{\left(\frac{\sqrt{N_{signal} + N_{background}}}{\epsilon \cdot \mathcal{L}}\right)^2 + \left(\frac{\sqrt{N_{background}}}{\epsilon \cdot \mathcal{L}}\right)^2} = \frac{\sqrt{N_{signal} + 2 \cdot N_{background}}}{\epsilon \cdot \mathcal{L}} \end{aligned} \tag{4.4}$$

$$\Delta\hat{\sigma}_{syst} = \sqrt{\left(\frac{\Delta N_{background}^{syst}}{\epsilon \cdot \mathcal{L}}\right)^2 + \left(\hat{\sigma} \cdot \frac{\Delta\epsilon}{\epsilon}\right)^2 + \left(\hat{\sigma} \cdot \frac{\Delta\mathcal{L}}{\mathcal{L}}\right)^2} \tag{4.5}$$

Equations 4.3 describes the uncertainties of the expected cross section $\Delta\hat{\sigma}$. The statistical uncertainty is fully described by Equation 4.4, while the choices for the systematic uncertainties in Equation 4.5 need to be clarified.

- Luminosity uncertainty $\Delta\mathcal{L}$:
  The uncertainty on the luminosity is estimated to be 2.8%. This value was obtained for 8 TeV in a similar way as described in Reference [43].

- Efficiency uncertainty $\Delta\epsilon$:
  The uncertainty on the efficiency consists of detector related uncertainties, which are jet-, photon-, electron- and muon-energy scale and energy resolution, as well as the b-tagging uncertainty. The value of the efficiency uncertainty depends on the choice of requirements and changes throughout the optimization. In general it is larger than the luminosity uncertainty.

- Background uncertainty $\Delta N^{syst}_{background}$:
  In addition to the statistical background uncertainty of $\sqrt{N_{background}}$, the systematic uncertainty on the background, due to the modeling of the MC samples, is estimated to be $0.5 \cdot N_{background}$. This is an assumption and it is suggested by the result from the 7 TeV $t\bar{t}\gamma$ analysis [22]. The background uncertainty is the largest contribution to the systematic uncertainties and also changes for each set of requirements.

Optimization procedure

The requirements that were optimized in this analysis are all photon-related quantities, as they have the largest impact on filtering the signal $t\bar{t}\gamma$ events. Since most of the requirements are expected to be uncorrelated, the optimization was done separately and not multidimensional. For the p_T-cone20 and E_T-cone40 isolation variables, that are expected to be highly correlated, a two-dimensional optimization was performed. The list of requirements being optimized for this analysis are:

- the minimum photon p_T
- the minimum ΔR of the photon and any jet
- the minimum ΔR of the photon and any lepton
- the maximum p_T-cone20 and E_T-cone40 values

The optimization is done in the order listed.
The initial values of the ΔR requirements are based on those used for the 7 TeV analysis [22]. For the photon p_T, p_T-cone20 and E_T-cone40 requirements the initial values are chosen according to the separation of the signal photons and photons from hadron decays. The ranges largely agree with the ones considered for photon reconstruction in ATLAS [42].

Photon p_T

Before doing the optimization a reasonable range of allowed values for each requirement has to be defined. For the photon p_T this is $15 - 60$ GeV. The generator level cut on the photon p_T is 10 GeV, however the precise reconstruction and calibration of photons at ATLAS is possible only for photons with $p_T > 15$ GeV. The upper end of 60 GeV is chosen arbitrarily, but with the intention not too loose too many events with photons radiated from the top quarks. The requirement for the photon p_T is increased by 5 GeV for each step in the optimization.

Table 4.1 summarizes the initial values for the requirements, which are not optimized yet as well as the range of the optimization for the photon's p_T.

Figure 4.3 shows the result of the optimization for the photon's p_T. It shows that the minimum value of 15 GeV is preferred, because it has the smallest expected relative uncertainty on the cross section. The optimization was done only at the highlighted points in steps of 5 GeV, connected with a red line for visualization purposes.

Requirement	Value
minimum photon p_{T}	15 – 60 GeV
minimum ΔR of the photon and any jet	0.5
minimum ΔR of the photon and any lepton	0.7
maximum p_{T}-cone20	2 GeV
maximum E_{T}-cone40	5 GeV

Table 4.1: Setup for the first part of the optimization of the event selection.

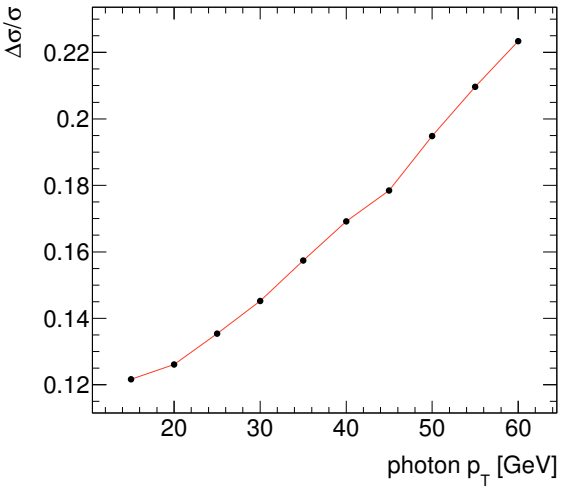

Figure 4.3: Relative uncertainty on the expected cross section $\Delta\hat{\sigma}/\sigma$ as a function of the photon's p_{T}.

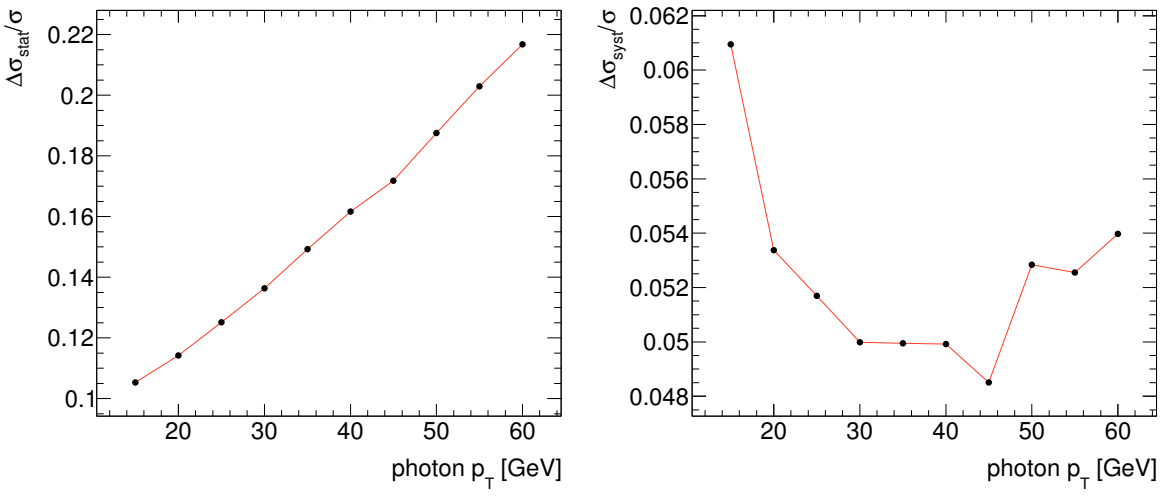

(a) Relative statistical uncertainty.

(b) Relative systematic uncertainty.

Figure 4.4: Expected relative statistical and systematic uncertainty on the cross section as a function of the photon's p_{T}.

Figure 4.4 shows the the optimization for the photon's p_T split into the statistical uncertainty (a) and the systematic uncertainty (b). By comparing the scales of the vertical axis of both figures, it can be seen that the statistical uncertainty has an impact of roughly 10 – 20%, while the systematic uncertainty has an impact of only 5 – 6%.

ΔR of the photon and any jet

The allowed range for the requirement on the ΔR of the photon and any jet for the optimization is between 0.4 (corresponding to the jet radius) and 1.0. Choosing a value that is too large will remove too many events in the selection, because the photon can be close to a jet in the detector by coincidence, without being radiated from it. The ΔR of the photon and any jet is optimized in steps of 0.05.

Requirement	Value
minimum photon p_T	15 GeV
minimum ΔR of the photon and any jet	0.4 – 1.0
minimum ΔR of the photon and any lepton	0.7
maximum p_T-cone20	2 GeV
maximum E_T-cone40	5 GeV

Table 4.2: Setup for the second part for the optimization of the event selection.

Table 4.2 shows the values for the different requirements for the second part of the optimization. The photon's p_T of 15 GeV has already been determined in the first part.

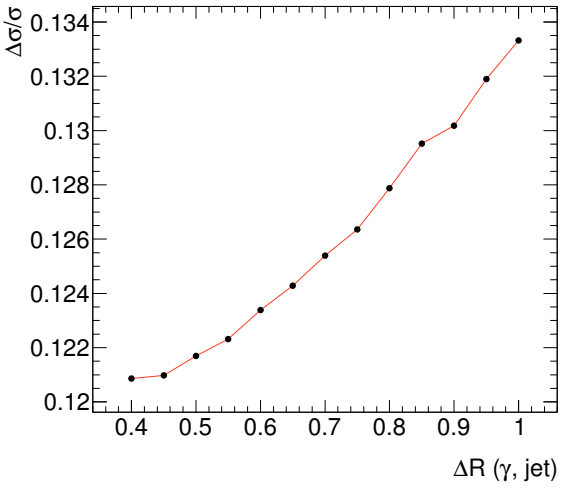

Figure 4.5: Expected relative uncertainty on the cross section $\Delta\hat{\sigma}/\sigma$ as a function of ΔR of the photon and any jet.

Figure 4.5 shows the result for the optimization for the ΔR of the photon and any jet. Similarly to the optimization of the photon's p_T, the smallest relative uncertainty can be achieved when using the lowest minimum requirement.

Figure 4.6 shows the the optimization for the ΔR of the photon and any jet split into the statistical uncertainty (a) and the systematic uncertainty (b). Again the total relative uncertainty is dominated by

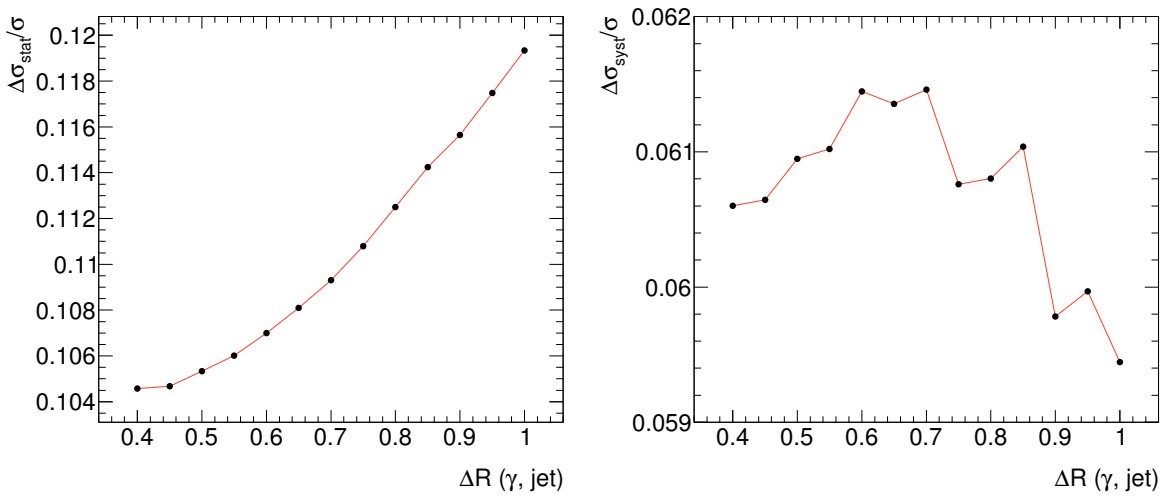

(a) Relative statistical uncertainty.

(b) Relative systematic uncertainty.

Figure 4.6: Expected relative statistical and systematic uncertainty on the cross section as a function of the ΔR of the photon and any jet.

the statistical uncertainty. Since the gain of decreasing the standard value of ΔR=0.5 [22] to the smaller value of 0.4 is negligible, the ΔR=0.5 is standard value is preferred.

ΔR of the photon and any lepton

The allowed range of the requirement on the ΔR of the photon and any lepton for the optimization is between 0.5 and 1.0. The minimum value of 0.5 is based on the conclusion of the optimization of the ΔR of the photon and any jet. The optimization of the ΔR of the photon and any lepton is done in steps of 0.05.

Requirement	Value
minimum photon p_{T}	15 GeV
minimum ΔR of the photon and any jet	0.5
minimum ΔR of the photon and any lepton	0.5 – 1.0
maximum p_{T}-cone20	2 GeV
maximum E_{T}-cone40	5 GeV

Table 4.3: Setup for the third part for the optimization of the event selection.

Table 4.3 shows the values for the different requirements for the third part of the optimization. The photon's p_{T} and the ΔR of the photon and any jet have been determined previously.

Figure 4.7 shows the result for the optimization for the ΔR of the photon and any lepton. Since this requirement is very similar in nature to the ΔR of the photon and any jet, the smallest relative uncertainty on the expected cross section is again at the loosest requirement, which allows the largest number of events to pass the selection.

Figure 4.8 shows the optimization for the ΔR of the photon and any lepton split into the statistical uncertainty (a) and the systematic uncertainty (b). The distributions for the ΔR of the photon and any

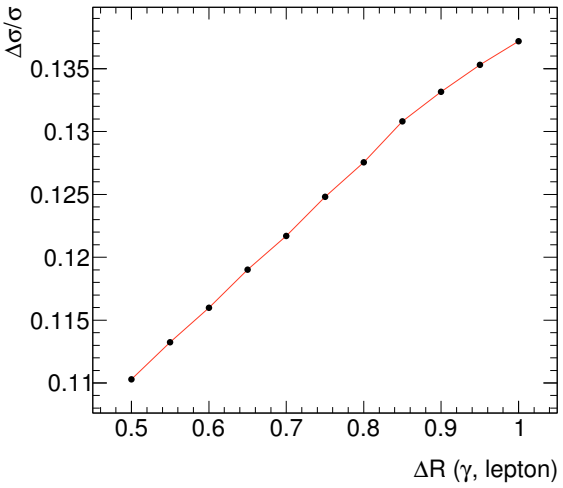

Figure 4.7: Expected relative uncertainty on the cross section $\Delta\hat{\sigma}/\sigma$ as a function of ΔR of the photon and any jet.

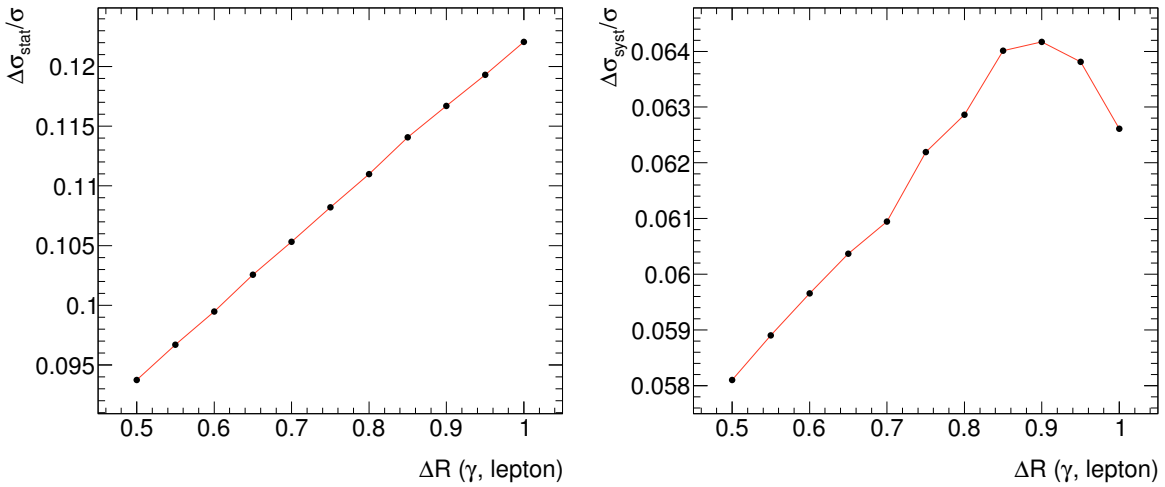

(a) Relative statistical uncertainty.

(b) Relative systematic uncertainty.

Figure 4.8: Expected relative statistical and systematic uncertainty on the cross section as a function of ΔR of the photon and any lepton.

lepton are not as flat as the corresponding distributions for the ΔR of the photon and any jet in Figure 4.5 and 4.6, however the lowest possible requirement is not chosen for the ΔR of the photon and any lepton, but the corresponding value of the 7 TeV analysis of $\Delta R = 0.7$ [22]. The same value was used in the single lepton study in Section 3 and necessary to reduce the contribution of photons close to leptons (see Figure 3.8a.

Summary of the first three parts of the optimization

For the one-dimensional optimizations of the photon's p_{T}, the ΔR of the photon and any jet and the ΔR of the photon and any lepton, the results are dominated by the statistical uncertainties, preferring the loosest possible requirements.

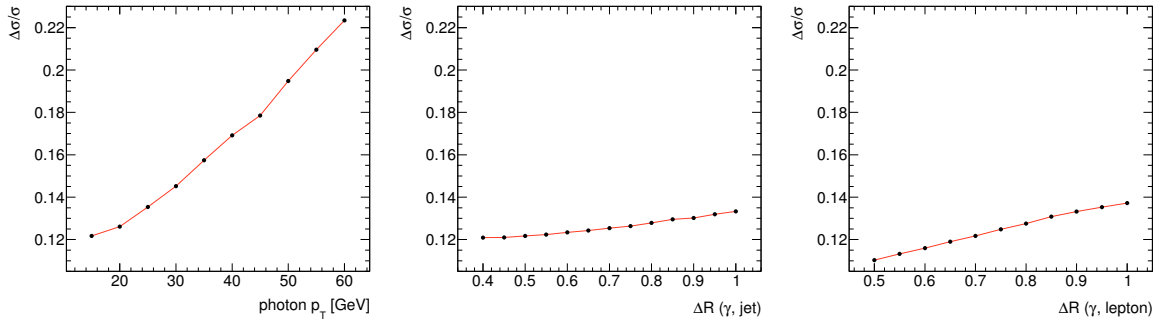

(a) First part of the optimization. (b) Second part of the optimization (c) Third part of the optimization.

Figure 4.9: Comparison of the results for the photon's p_{T}, the ΔR of the photon and any jet and the ΔR of the photon and any lepton.

Figure 4.9 shows the results for the first three part of the optimization. All Figures use the same scale on the vertical axis, showing how large the impact on each of these requirements are. Since the relative uncertainty is less affected by the ΔR requirements, the choice of using the values from the 7 TeV analysis [22] is reasonable.

Two dimensional optimization of p_{T}-cone20 and E_{T}-cone40

Since p_{T}-cone20 and E_{T}-cone40 are expected to be correlated, this final part of the optimization is done in two dimensions. For the allowed ranges the shape of the distributions for p_{T}-cone20 and E_{T}-cone40 are considered.

Figure 4.10 shows the distributions of p_{T}-cone20 and E_{T}-cone40 for both the $t\bar{t}\gamma$ and the $t\bar{t}$ MC samples. In the figures the entries are normalized to 1. Instead of the whole set of background samples, only the main background is shown here. Both p_{T}-cone20 and E_{T}-cone40 show a good separation between signal and background. Based on the distributions in Figure 4.10 the chosen regions for the two-dimensional optimization are $1 - 5$ GeV for p_{T}-cone20 and $2 - 10$ GeV for E_{T}-cone40. To have a symmetrical two-dimensional optimization, p_{T}-cone20 is optimized in steps of 0.5 GeV and E_{T}-cone40 is optimized in steps of 1 GeV.

Table 4.4 shows the values for the requirements obtained by the optimization so far, as well as the allowed range for the p_{T}-cone20 and E_{T}-cone40 requirements, which are optimized in this final part.

Figure 4.11 shows the result for the two-dimensional optimization of p_{T}-cone20 and E_{T}-cone40. In contrast to the one-dimensional optimizations of the photon's p_{T}, the ΔR of the photon and any jet

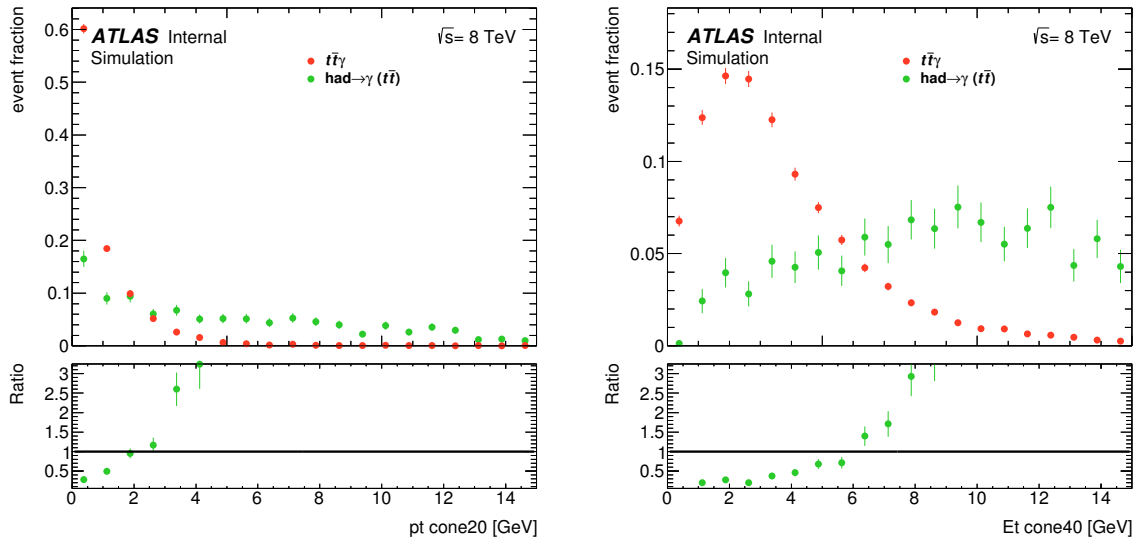

(a) p_{T}-cone20. (b) E_{T}-cone40.

Figure 4.10: Distributions of p_{T}-cone20 and E_{T}-cone40 for the signal and main background MC sample.

Requirement	Value
minimum photon p_{T}	15 GeV
minimum ΔR of the photon and any jet	0.5
minimum ΔR of the photon and any lepton	0.7
maximum p_{T}-cone20	1 – 5 GeV
maximum E_{T}-cone40	2 – 10 GeV

Table 4.4: Setup for the final part for the optimization of the event selection.

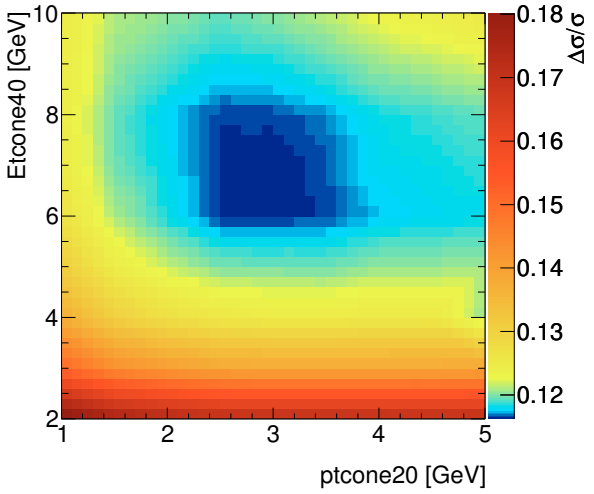

Figure 4.11: Expected relative uncertainty on the cross section $\Delta\hat{\sigma}$ as a function of p_{T}-cone20 and E_{T}-cone40.

and the ΔR of the photon and any lepton, the loosest possible requirement does not yield the minimal uncertainty. The preferred set of values can be found at p_{T}-cone20 of 3 GeV and E_{T}-cone40 of 7 GeV.

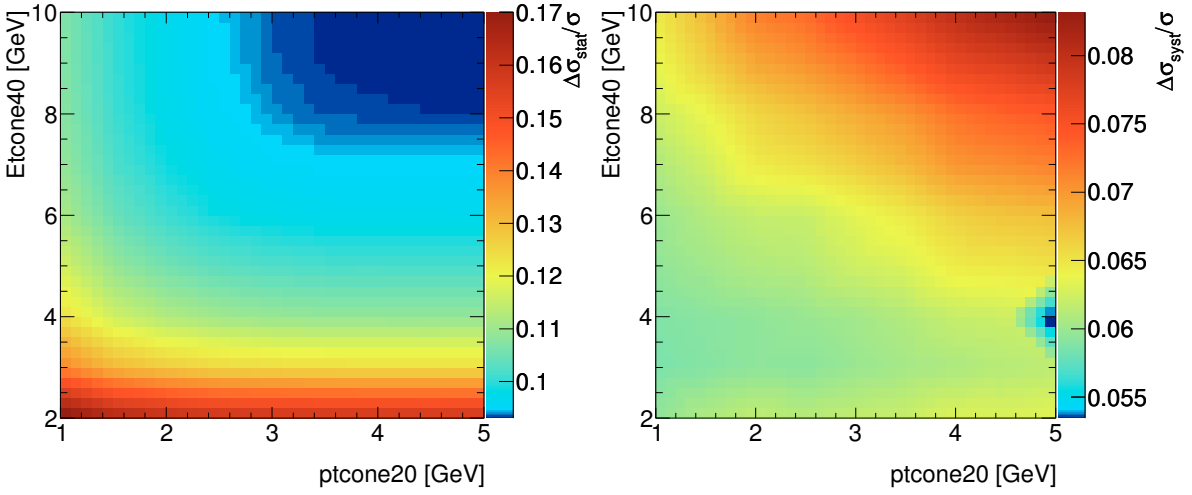

(a) Relative statistical uncertainty.

(b) Relative systematic uncertainty.

Figure 4.12: Expected relative statistical and systematic uncertainty on the cross section as a function of p_{T}-cone20 and E_{T}-cone40.

Figure 4.12 shows the two-dimensional optimization of p_{T}-cone20 and E_{T}-cone40 split into the statistical and the systematic uncertainty. Even though this part of the optimization is also dominated by the statistical uncertainty, the relative contribution of the systematic uncertainty is increased compared to the one-dimensional optimizations. Both distributions of the statistical and the systematic uncertainty have their minimum at the right border of the p_{T}-cone20 scale at 5 GeV. However extending this trend does not continue by extending the p_{T}-cone20 scale. Additionally the minimum of the total relative uncertainty in Figure 4.11 is at a p_{T}-cone20 of 3 GeV. When allowing any value for p_{T}-cone20 and E_{T}-cone40, so essentially removing their requirements, the relative uncertainty rises to a value of 22%, which is outside of the scale in Figure 4.11.

Requirement	Value
minimum photon p_{T}	15 GeV
minimum ΔR of the photon and any jet	0.5
minimum ΔR of the photon and any lepton	0.7
maximum p_{T}-cone20	3 GeV
maximum E_{T}-cone40	7 GeV

Table 4.5: Result of the complete optimization of the event selection.

Table 4.5 shows the result of the optimization of the event selection for all considered cuts. For the used optimization procedure and considered systematic uncertainties, the only requirements, which do not prefer the loosest possible cuts are p_{T}-cone20 and E_{T}-cone40. However the optimization of these two requirements also has the largest impact on the systematic uncertainties.

4.5 Results

4.5.1 Kinematic distributions using the optimal requirements

With the optimization providing the optimal set of requirements, as described in Table 4.5, the kinematic distributions need to be checked, to ensure a good data and MC agreement. If the data and the MC would not match in the stack plots, the list of considered backgrounds for this analysis might be incomplete and the modeling of the signal and background MC samples has to be checked thoroughly.

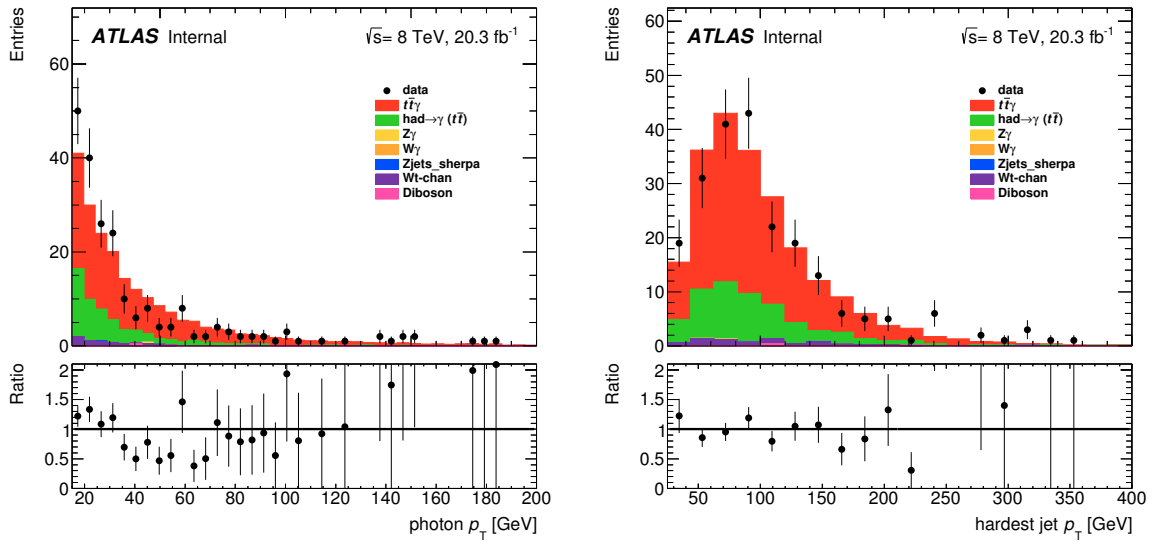

(a) Photon p_{T}.

(b) Hardest jet p_{T}.

Figure 4.13: Photon and hardest jet p_{T} distributions just before applying the p_{T}-cone20 and E_{T}-cone40 requirements.

Figure 4.13 shows the p_{T} distributions of the photon and the hardest jet before applying the p_{T}-cone20 and E_{T}-cone40 cuts in the event selection. The data and MC agreement is good, but a lot of events were removed in the event selection in comparison to Figure 4.2. The shown histograms are using the ΔR cuts obtained in the optimization.

Figure 4.14 shows the p_{T} distributions of the photon and the hardest jet after the full event selection is applied. The two distributions show that the data is still described well by the simulation samples. The optimization of the event selection has helped to reduce the background, since the signal MC sample is the dominant contribution.

Sample	Number of events
data	140
signal MC	132 ± 12
background MC	13 ± 4 (stat.) ± 7 (syst.)

Table 4.6: Amount of events remaining after the full event selection.

Table 4.6 shows the number of events remaining for the data, signal and background samples after applying the full event selection with the requirements obtained from the optimization. The uncertainties

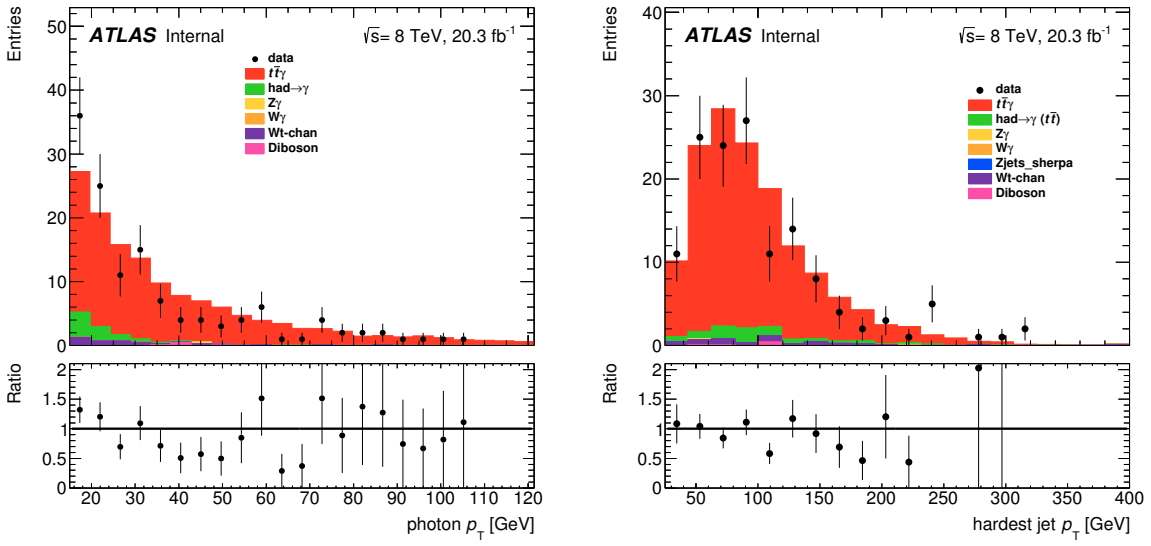

(a) Photon p_{T}.

(b) Hardest jet p_{T}.

Figure 4.14: Photon and hardest jet p_{T} distributions after the full event selection.

for the signal MC are statistical. The signal-to-background ratio is ~10, which is significantly higher than in many other ATLAS analyses.

4.5.2 Cross section measurement

Having checked that the data and MC agreement is good for the requirements obtained from the optimization, the measurement of the cross section σ can be done.

The generator cuts used for this analysis are:

- minimum photon p_{T} of 10 GeV
- maximum photon $|\eta| = 5$
- minimum p_{T} for one charged lepton of 15 GeV
- maximum lepton $|\eta| = 5$
- minimum $\Delta R(\gamma, \ell)$ of 0.2
- minimum $\Delta R(\gamma, \mathrm{j})$ of 0.2

The cross section result is obtained by only using dilepton events, although the samples contained both single lepton and dilepton events (lepton = e, μ, τ), the single lepton events have not been looked at. Hence the efficiency ϵ is evaluated as fraction of events passing the eμ-channel selection, while the cross section is normalized to the single lepton and dilepton channel. The measured cross section is evaluated as:

$$\sigma = \frac{\mathrm{N_{data}} - \mathrm{N_{background}}}{\epsilon \cdot \mathcal{L}} \tag{4.6}$$

with uncertainties:

$$\Delta\sigma_{\text{stat}} = \sqrt{\left(\frac{\Delta N_{\text{data}}}{\epsilon \cdot \mathcal{L}}\right)^2 + \left(\frac{\Delta N_{\text{background}}}{\epsilon \cdot \mathcal{L}}\right)^2} = \frac{\sqrt{N_{\text{data}} + N_{\text{background}}}}{\epsilon \cdot \mathcal{L}} \tag{4.7}$$

$$\Delta\sigma_{\text{syst}} = \sqrt{\left(\frac{\Delta N^{\text{syst}}_{\text{background}}}{\epsilon \cdot \mathcal{L}}\right)^2 + \left(\sigma \cdot \frac{\Delta\epsilon}{\epsilon}\right)^2 + \left(\sigma \cdot \frac{\Delta\mathcal{L}}{\mathcal{L}}\right)^2} \tag{4.8}$$

Equation 4.6 shows the definition of the cross section σ. The difference to the expected cross section $\hat{\sigma}$, defined in Equation 4.1 is the usage of N_{data} instead of $N_{\text{signal}} + N_{\text{background}}$ in the numerator, which then expands to the corresponding uncertainties in equations 4.7 and 4.8. The systematic uncertainties are obtained in the the same way as described in Section 4.4.1.
The result of the measurement is:

$$\sigma_{t\bar{t}\gamma} \times \text{BR}(t\bar{t}\gamma \rightarrow \text{single lepton or dilepton}) = 2.71 \ \pm \ 0.26\,(\text{stat.}) \ \pm \ 0.22\,(\text{syst.})\ \text{pb} \tag{4.9}$$

Source	Uncertainty [%]
Background modeling	5.3
Photon modeling	1.2
Lepton modeling	0.4
Jet modeling	1.0
E_T^{miss} modeling	$< 10^{-3}$
b-tagging	5.7
Luminosity	2.8
total	8.0

Table 4.7: Systematic uncertainties of the cross section measurement.

Table 4.7 lists all contributions to the systematic uncertainties. The largest contributions are from the *b*-tagging scale factors and from the background modeling. The contribution from the background modeling is rather large, because the uncertainty on the background modeling was assumed to be 50% as in the 7 TeV analysis [22]. Using a dedicated estimate for the dilepton channel, this source of the uncertainty could be in principle reduced. Signal modeling uncertainties were neglected for the measurement due to the lack of convenient samples to estimate it. In the 7 TeV analysis the relative uncertainty, due to the signal modeling was determined to be 8.4%, while the dominant contribution in this analysis was the jet modeling, with a relative uncertainty of 16.6% [22].

Table 4.8 shows the result of the cross section measurement in comparison to results obtained by other measurements. The result of this thesis and the SM theory prediction [21] quote a cross section which is normalized to the single lepton and the dilepton channel. The 7 TeV analysis from ATLAS quotes a cross section, which is normalized to the single lepton channel [22] and the preliminary result from CMS at 8 TeV quotes an inclusive cross section [23].

Measurement	Value	Channel used
Result at 8 TeV (this thesis)	2.6 ± 0.3 (stat.) ± 0.2 (syst.) pb	dilepton
NLO theory prediction at 8 TeV [21]	2.2 ± 0.3 pb	dilepton
ATLAS at 7 TeV [22]	63 ± 8 (stat.) $^{+17}_{-13}$ (syst.) ± 1 (lumi.) fb	single lepton
CMS at 8 TeV [23]	2.4 ± 0.2 (stat.) ± 0.6 (syst.) pb	single lepton

Table 4.8: Comparison of different $t\bar{t}\gamma$ cross section results.

Compatibility of the result to the SM theory prediction

The theoretical prediction for the SM cross section in Table 4.8 was done in the single lepton and dilepton channels, as the result in Equation 4.9. For a direct comparison a total uncertainty is more useful than an uncertainty split into statistical and systematic uncertainty.

$$\begin{aligned} \sigma_{\text{thesis}} &= 2.6 \ \pm \ 0.3 \text{ (stat.)} \ \pm \ 0.2 \text{ (syst.) pb} = 2.6 \ \pm \ 0.3 \text{ pb} \\ \sigma_{\text{theory}} &= 2.2 \ \pm \ 0.3 \text{ pb} \end{aligned} \tag{4.10}$$

Equation 4.10 shows the result of the measurement with the total uncertainty and the corresponding theory prediction. The theory prediction was obtained with the same methods as mentioned in Reference [21]. The corresponding factors were applied to normalize the theory prediction to the single lepton and dilepton channel. To check the compatibility of the measurement and the theory prediction, the sigma range of the two values can be compared.

$$\text{Compatibility} = \frac{|\sigma_{\text{thesis}} - \sigma_{\text{theory}}|}{\sqrt{\Delta\sigma^2_{\text{thesis}} + \Delta\sigma^2_{\text{theory}}}} \tag{4.11}$$

Equation 4.11 shows the definition of the compatibility of two values. For the theory value and the measurement the compatibility is 0.9, which falls inside the one-sigma-range. Therefore the SM theory prediction and the measurement are compatible.

Compatibility of the result to the measurement of ATLAS and CMS

The measurement from ATLAS quotes the $t\bar{t}\gamma$ cross section in the single lepton channel (ℓ = e, μ) only, the measurement from CMS quotes an inclusive $t\bar{t}\gamma$ cross section, while the result of this thesis is quoted for both the single lepton and dilepton channel (ℓ = e, μ, τ). Additionally the results are for different centre-of-mass-energies, with the ATLAS result being for 7 TeV and the CMS and this thesis's results being for 8 TeV.

$$\begin{aligned} \sigma_{\text{thesis}} &= 2.6 \ \pm \ 0.3 \text{ (stat.)} \ \pm \ 0.2 \text{ (syst.) pb}, \ \ p_{\text{T}}^{\gamma} > 15 \text{ GeV} \\ \sigma_{\text{ATLAS}} &= 63 \ \pm \ 8 \text{ (stat.)} \, ^{+17}_{-13} \text{ (syst.)} \ \pm \ 1 \text{ (lumi.) fb}, \ \ E_{\text{T}}^{\gamma} > 20 \text{ GeV} \\ \sigma_{\text{CMS}} &= 2.4 \ \pm \ 0.2 \text{ (stat.)} \ \pm \ 0.6 \text{ (syst.) pb}, \ \ p_{\text{T}}^{\gamma} > 20 \text{ GeV} \end{aligned} \tag{4.12}$$

Equation 4.12 shows the result of ATLAS, CMS and this thesis for the cross section with their uncertainties. A direct compatibility like in Equation 4.11 is not sensible because the three cross sections are quoted for different channels. Additionally the requirement on the photon are different than the one

for this thesis. The absolute value of the CMS measurement is of comparable size to the measurement of the thesis, although CMS quotes an inclusive (fiducial) measurement. Additionally the result from ATLAS obtained in the single lepton channel is more than a magnitude smaller. Both discrepancies can be explained with the different requirements on the photon for ATLAS and CMS, as shown in Equation 4.12. Although the absolute values of the cross sections are not directly comparable, a comparison of the relative uncertainties is possible:

$$\begin{aligned} \Delta\sigma_{\text{thesis}}/\sigma_{\text{thesis}} &= 10\%\ (\text{stat.})\ \pm 8\%\ (\text{syst.}) = 13\%\ (\text{tot.}) \\ \Delta\sigma_{\text{ATLAS}}/\sigma_{\text{ATLAS}} &= 14\%\ (\text{stat.})\ \pm 27\%\ (\text{syst.}) = 30\%\ (\text{tot.}) \\ \Delta\sigma_{\text{CMS}}/\sigma_{\text{CMS}} &= 8\%\ (\text{stat.})\ \pm 25\%\ (\text{syst.}) = 26\%\ (\text{tot.}) \end{aligned} \tag{4.13}$$

Equation 4.13 shows the relative uncertainties in percent for the measurements of ATLAS, CMS and this thesis. While the statistical uncertainties are comparable, the relative systematic uncertainties are significantly lower when using dilepton $e\mu$ events. For both CMS and this thesis, the systematic uncertainty is dominated by the background modeling, while for the ATLAS measurement the dominating contribution is the jet modeling. The result of CMS and ATLAS are in the one-sigma-range to the theory prediction, cited in their references [22] and [23]. Since the agreement of the cross section of this thesis and the theory prediction is also in the one-sigma-range, the compatibility to the other measurements by ATLAS and CMS is given.

CHAPTER 5

Conclusion

In this thesis two $t\bar{t}\gamma$ studies were performed. In the first study, a search for the most suitable MC generator in the single-lepton channel was presented. In particular, the performance of production samples (in LO and NLO) and decay samples (in LO only) were compared. For the p_{T} of the photon, the production samples in both LO and NLO behaved (very) similarly, while the final state radiation in the decay sample dominated for low values of p_{T}. Additionally the performance of different parton shower and different QED emission generators were tested. In conclusion the LO decay sample, which uses MadGraph and Pythia is the preferred one for 8 TeV and will be used for the upcoming 8 TeV analysis in ATLAS.
In the second study a cross section measurement, using $t\bar{t}\gamma$ dilepton events at 8 TeV, obtained by the ATLAS detector, was presented. The strategy was to do a cut-and-count analysis with the photon related requirements being optimized, for the lowest expected uncertainty on the cross section. The result was normalized to both the single lepton and dilepton channel, since the samples used for this analysis contained both types of events. The result obtained in this analysis is:

$$\sigma_{t\bar{t}\gamma} \times \mathrm{BR}(t\bar{t}\gamma \rightarrow \text{single lepton or dilepton}) = 2.6 \ \pm \ 0.3 \ (\text{stat.}) \ \pm \ 0.2 \ (\text{syst.}) \ \text{pb}$$

The result is within a one sigma range of the corresponding theory prediction. The relative systematic uncertainty of 8% is significantly lower than the corresponding systematic uncertainties for the cross section measurements done by ATLAS and CMS. The $t\bar{t}\gamma$ process will be investigated further for the ATLAS 8 TeV publication and with the new data at 13 TeV, which is continued to be collected in 2016.

APPENDIX A

Useful information

A.1 Technical information about the MC samples

A.1.1 MadGraph cards

In Section 3.1.2 the settings for the samples used in the MC analysis are introduced. The MadGraph card shows the exact settings for the processed sample and is divided into multiple subcards.

```
<LesHouchesEvents version="1.0">
<header>
<!--
#*****************************************************************
#                                                                *
#                          MadGraph5_aMC@NLO                     *
#                                                                *
#                              Going Beyond                      *
#                                                                *
#                     http://madgraph.hep.uiuc.edu               *
#                     http://madgraph.phys.ucl.ac.be             *
#                     http://amcatnlo.cern.ch                    *
#                                                                *
#                       The MadGraph5_aMC@NLO team               *
#                                                                *
#.................................................................*
#                                                                *
# This file contains all the information necessary to reproduce  *
# the events generated:                                          *
#                                                                *
# 1. software version                                            *
# 2. proc_card          : code generation info including model   *
# 3. param_card         : model primary parameters in the LH format *
# 4. run_card           : running parameters (collider and cuts) *
#                                                                *
#                                                                *
#*****************************************************************
-->
<MGVersion>
#5.2.1.2
</MGVersion>
<MG5ProcCard>
#*************************************************************
#*                        MadGraph5_aMC@NLO                  *
#*                                                           *
#*                *                       *                  *
#*                  *         * *         *                  *
```

```
#*                        * * * * 5 * * * *                   *
#*                     *         * *         *                *
#*                  *                           *             *
#*                                                            *
#*                                                            *
#*           VERSION 2.1.0                2014-02-21          *
#*                                                            *
#*     The MadGraph5_aMC@NLO Development Team - Find us at    *
#*     https://server06.fynu.ucl.ac.be/projects/madgraph      *
#*                                                            *
#************************************************************
#*                                                            *
#*                Command File for MadGraph5_aMC@NLO          *
#*                                                            *
#*      run as ./bin/mg5_aMC  filename                        *
#*                                                            *
#************************************************************
set group_subprocesses Auto
set ignore_six_quark_processes False
set loop_optimized_output True
set gauge unitary
set complex_mass_scheme False
import model sm
define p = g u c d s u~ c~ d~ s~
define l+ = e+ mu+ ta+
define l- = e- mu- ta-
define vl = ve vm vt
define vl~ = ve~ vm~ vt~
define uc = u c
define uc~ = u~ c~
define ds = d s
define ds~ = d~ s~
generate p p > t t~ a, (t > W+ b, W+ > uc ds~), (t~ > W- b~, W- > l- vl~)
add process p p > t t~ a, (t > W+ b, W+ > l+ vl), (t~ > W- b~, W- > ds uc~)
add process p p > t t~ a, (t > W+ b, W+ > l+ vl), (t~ > W- b~, W- > l- vl~)
output ttbargammanoallhad_2part
</MG5ProcCard>
<MGProcCard>
#*********************************************************************
#                        MadGraph/MadEvent                           *
#                     http://madgraph.hep.uiuc.edu                   *
#                                                                    *
#                           proc_card.dat                            *
#*********************************************************************
#                                                                    *
#            This Files is generated by MADGRAPH 5                   *
#                                                                    *
# WARNING: This Files is generated for MADEVENT (compatibility issue)*
#          This files is NOT a valid MG4 proc_card.dat               *
#          Running this in MG4 will NEVER reproduce the result of MG5*
#                                                                    *
#*********************************************************************
#*********************************************************************
# Process(es) requested : mg2 input                                  *
#*********************************************************************
# Begin PROCESS # This is TAG. Do not modify this line
p p > t t~ a , (t > W+ b , W+ > uc ds~) , (t~ > W- b~ , W- > l- vl~)          #
```

```
    Process
# Be carefull the coupling are here in MG5 convention

end_coup           # End the couplings input

done               # this tells MG there are no more procs
# End PROCESS  # This is TAG. Do not modify this line
#*********************************************************************
# Model information                                                  *
#*********************************************************************
# Begin MODEL  # This is TAG. Do not modify this line
sm
# End   MODEL  # This is TAG. Do not modify this line
#*********************************************************************
# Start multiparticle definitions                                    *
#*********************************************************************
# Begin MULTIPARTICLES # This is TAG. Do not modify this line

# End  MULTIPARTICLES # This is TAG. Do not modify this line
</MGProcCard>
<MGRunCard>
#*********************************************************************
#                        MadGraph5_aMC@NLO                           *
#                                                                    *
#                      run_card.dat MadEvent                         *
#                                                                    *
#  This file is used to set the parameters of the run.               *
#                                                                    *
#  Some notation/conventions:                                        *
#                                                                    *
#   Lines starting with a '# ' are info or comments                  *
#                                                                    *
#   mind the format:   value    = variable     ! comment             *
#*********************************************************************
#
#*******************
# Running parameters
#*******************
#
#*********************************************************************
# Tag name for the run (one word)                                    *
#*********************************************************************
  tag_1     = run_tag ! name of the run
#*********************************************************************
# Run to generate the grid pack                                      *
#*********************************************************************
  .false.     = gridpack  !True = setting up the grid pack
#*********************************************************************
# Number of events and rnd seed                                      *
# Warning: Do not generate more than 1M events in a single run       *
# If you want to run Pythia, avoid more than 50k events in a run.    *
#*********************************************************************
   200000 = nevents ! Number of unweighted events requested
 21 = iseed   ! rnd seed (0=assigned automatically=default))
#*********************************************************************
# Collider type and energy                                           *
# lpp: 0=No PDF, 1=proton, -1=antiproton, 2=photon from proton,      *
```

```
#                                        3=photon from electron      *
#*********************************************************************
        1      = lpp1     ! beam 1 type
        1      = lpp2     ! beam 2 type
     4000      = ebeam1   ! beam 1 total energy in GeV
     4000      = ebeam2   ! beam 2 total energy in GeV
#*********************************************************************
# Beam polarization from -100 (left-handed) to 100 (right-handed)     *
#*********************************************************************
        0      = polbeam1 ! beam polarization for beam 1
        0      = polbeam2 ! beam polarization for beam 2
#*********************************************************************
# PDF CHOICE: this automatically fixes also alpha_s and its evol.     *
#*********************************************************************
 'cteq6l1'     = pdlabel     ! PDF set
#*********************************************************************
# Renormalization and factorization scales                            *
#*********************************************************************
 T        = fixed_ren_scale  ! if .true. use fixed ren scale
 T        = fixed_fac_scale  ! if .true. use fixed fac scale
 345.0    = scale            ! fixed ren scale
 345.0    = dsqrt_q2fact1    ! fixed fact scale for pdf1
 345.0    = dsqrt_q2fact2    ! fixed fact scale for pdf2
 1        = scalefact        ! scale factor for event-by-event scales
#*********************************************************************
# Matching - Warning! ickkw > 1 is still beta
#*********************************************************************
 0        = ickkw            ! 0 no matching, 1 MLM, 2 CKKW matching
 1        = highestmult      ! for ickkw=2, highest mult group
 1        = ktscheme         ! for ickkw=1, 1 Durham kT, 2 Pythia pTE
 1        = alpsfact         ! scale factor for QCD emission vx
 F        = chcluster        ! cluster only according to channel diag
 T        = pdfwgt           ! for ickkw=1, perform pdf reweighting
 5        = asrwgtflavor     ! highest quark flavor for a_s reweight
 T        = clusinfo         ! include clustering tag in output
 1.0      = lhe_version       ! Change the way clustering information pass to
    shower.
#*********************************************************************
#*********************************************************
#
#*********************************************************
# Automatic ptj and mjj cuts if xqcut > 0
# (turn off for VBF and single top processes)
#*********************************************************
   T  = auto_ptj_mjj  ! Automatic setting of ptj and mjj
#*********************************************************
#
#*********************************
# BW cutoff (M+/-bwcutoff*Gamma)
#*********************************
  15  = bwcutoff      ! (M+/-bwcutoff*Gamma)
#*********************************************************
# Apply pt/E/eta/dr/mij cuts on decay products or not
# (note that etmiss/ptll/ptheavy/ht/sorted cuts always apply)
#*********************************************************
   T  = cut_decays    ! Cut decay products
#*********************************************************
```

```
# Number of helicities to sum per event (0 = all helicities)
# 0 gives more stable result, but longer run time (needed for
# long decay chains e.g.).
# Use >=2 if most helicities contribute, e.g. pure QCD.
#*********************************************************
   0  = nhel          ! Number of helicities used per event
#*******************
# Standard Cuts
#*******************
#
#*********************************************************************
# Minimum and maximum pt's (for max, -1 means no cut)                 *
#*********************************************************************
  0  = ptj       ! minimum pt for the jets
  0  = ptb       ! minimum pt for the b
 10  = pta       ! minimum pt for the photons
  0  = ptl       ! minimum pt for the charged leptons
  0  = misset    ! minimum missing Et (sum of neutrino's momenta)
  0  = ptheavy   ! minimum pt for one heavy final state
 1.0 = ptonium   ! minimum pt for the quarkonium states
 -1  = ptjmax    ! maximum pt for the jets
 -1  = ptbmax    ! maximum pt for the b
 -1  = ptamax    ! maximum pt for the photons
 -1  = ptlmax    ! maximum pt for the charged leptons
 -1  = missetmax ! maximum missing Et (sum of neutrino's momenta)
#*********************************************************************
# Minimum and maximum E's (in the center of mass frame)               *
#*********************************************************************
  0  = ej      ! minimum E for the jets
  0  = eb      ! minimum E for the b
  0  = ea      ! minimum E for the photons
  0  = el      ! minimum E for the charged leptons
 -1   = ejmax ! maximum E for the jets
 -1   = ebmax ! maximum E for the b
 -1   = eamax ! maximum E for the photons
 -1   = elmax ! maximum E for the charged leptons
#*********************************************************************
# Maximum and minimum absolute rapidity (for max, -1 means no cut)    *
#*********************************************************************
  -1  = etaj     ! max rap for the jets
  -1  = etab     ! max rap for the b
  -1  = etaa     ! max rap for the photons
  -1  = etal     ! max rap for the charged leptons
 0.6  = etaonium ! max rap for the quarkonium states
   0  = etajmin ! min rap for the jets
   0  = etabmin ! min rap for the b
   0  = etaamin ! min rap for the photons
   0  = etalmin ! main rap for the charged leptons
#*********************************************************************
# Minimum and maximum DeltaR distance                                 *
#*********************************************************************
 0 = drjj     ! min distance between jets
 0   = drbb     ! min distance between b's
 0  = drll     ! min distance between leptons
 0  = draa     ! min distance between gammas
 0   = drbj     ! min distance between b and jet
 0.2 = draj     ! min distance between gamma and jet
```

```
 0 = drjl    ! min distance between jet and lepton
 0   = drab    ! min distance between gamma and b
 0   = drbl    ! min distance between b and lepton
 0.2 = dral    ! min distance between gamma and lepton
 -1  = drjjmax ! max distance between jets
 -1  = drbbmax ! max distance between b's
 -1  = drllmax ! max distance between leptons
 -1  = draamax ! max distance between gammas
 -1  = drbjmax ! max distance between b and jet
 -1  = drajmax ! max distance between gamma and jet
 -1  = drjlmax ! max distance between jet and lepton
 -1  = drabmax ! max distance between gamma and b
 -1  = drblmax ! max distance between b and lepton
 -1  = dralmax ! maxdistance between gamma and lepton
#*********************************************************************
# Minimum and maximum invariant mass for pairs                       *
# WARNING: for four lepton final state mmll cut require to have      *
#          different lepton masses for each flavor!                  *
#*********************************************************************
 0   = mmjj    ! min invariant mass of a jet pair
 0   = mmbb    ! min invariant mass of a b pair
 0   = mmaa    ! min invariant mass of gamma gamma pair
 0   = mmll    ! min invariant mass of l+l- (same flavour) lepton pair
 -1  = mmjjmax ! max invariant mass of a jet pair
 -1  = mmbbmax ! max invariant mass of a b pair
 -1  = mmaamax ! max invariant mass of gamma gamma pair
 -1  = mmllmax ! max invariant mass of l+l- (same flavour) lepton pair
#*********************************************************************
# Minimum and maximum invariant mass for all letpons                 *
#*********************************************************************
 0   = mmnl    ! min invariant mass for all letpons (l+- and vl)
 -1  = mmnlmax ! max invariant mass for all letpons (l+- and vl)
#*********************************************************************
# Minimum and maximum pt for 4-momenta sum of leptons                *
#*********************************************************************
 0   = ptllmin  ! Minimum pt for 4-momenta sum of leptons(l and vl)
 -1  = ptllmax  ! Maximum pt for 4-momenta sum of leptons(l and vl)
#*********************************************************************
# Inclusive cuts                                                     *
#*********************************************************************
 0  = xptj ! minimum pt for at least one jet
 0  = xptb ! minimum pt for at least one b
 0  = xpta ! minimum pt for at least one photon
 15.0  = xptl ! minimum pt for at least one charged lepton
#*********************************************************************
# Control the pt's of the jets sorted by pt                          *
#*********************************************************************
 0   = ptj1min ! minimum pt for the leading jet in pt
 0   = ptj2min ! minimum pt for the second jet in pt
 0   = ptj3min ! minimum pt for the third jet in pt
 0   = ptj4min ! minimum pt for the fourth jet in pt
 -1  = ptj1max ! maximum pt for the leading jet in pt
 -1  = ptj2max ! maximum pt for the second jet in pt
 -1  = ptj3max ! maximum pt for the third jet in pt
 -1  = ptj4max ! maximum pt for the fourth jet in pt
 0   = cutuse  ! reject event if fails any (0) / all (1) jet pt cuts
#*********************************************************************
```

```
# Control the pt's of leptons sorted by pt                    *
#*************************************************************
 0   = ptl1min ! minimum pt for the leading lepton in pt
 0   = ptl2min ! minimum pt for the second lepton in pt
 0   = ptl3min ! minimum pt for the third lepton in pt
 0   = ptl4min ! minimum pt for the fourth lepton in pt
 -1  = ptl1max ! maximum pt for the leading lepton in pt
 -1  = ptl2max ! maximum pt for the second lepton in pt
 -1  = ptl3max ! maximum pt for the third lepton in pt
 -1  = ptl4max ! maximum pt for the fourth lepton in pt
#*************************************************************
# Control the Ht(k)=Sum of k leading jets                     *
#*************************************************************
 0   = htjmin ! minimum jet HT=Sum(jet pt)
 -1  = htjmax ! maximum jet HT=Sum(jet pt)
 0   = ihtmin  !inclusive Ht for all partons (including b)
 -1  = ihtmax  !inclusive Ht for all partons (including b)
 0   = ht2min ! minimum Ht for the two leading jets
 0   = ht3min ! minimum Ht for the three leading jets
 0   = ht4min ! minimum Ht for the four leading jets
 -1  = ht2max ! maximum Ht for the two leading jets
 -1  = ht3max ! maximum Ht for the three leading jets
 -1  = ht4max ! maximum Ht for the four leading jets
#*************************************************************
# Photon-isolation cuts, according to hep-ph/9801442          *
# When ptgmin=0, all the other parameters are ignored         *
# When ptgmin>0, pta and draj are not going to be used        *
#*************************************************************
   0 = ptgmin ! Min photon transverse momentum
 0.4 = R0gamma ! Radius of isolation code
 1.0 = xn ! n parameter of eq.(3.4) in hep-ph/9801442
 1.0 = epsgamma ! epsilon_gamma parameter of eq.(3.4) in hep-ph/9801442
 .true. = isoEM ! isolate photons from EM energy (photons and leptons)
#*************************************************************
# WBF cuts                                                    *
#*************************************************************
 0   = xetamin ! minimum rapidity for two jets in the WBF case
 0   = deltaeta ! minimum rapidity for two jets in the WBF case
#*************************************************************
# KT DURHAM CUT                                               *
#*************************************************************
 -1    =  ktdurham
 0.4   =  dparameter
#*************************************************************
# maximal pdg code for quark to be considered as a light jet  *
# (otherwise b cuts are applied)                              *
#*************************************************************
 4 = maxjetflavor    ! Maximum jet pdg code
#*************************************************************
# Jet measure cuts                                            *
#*************************************************************
 0   = xqcut   ! minimum kt jet measure between partons
#*************************************************************
#
#*************************************************************
# Store info for systematics studies                          *
# WARNING: If use_syst is T, matched Pythia output is         *
```

```
#           meaningful ONLY if plotted taking matchscale                *
#           reweighting into account!                                   *
#*********************************************************************
   F  = use_syst       ! Enable systematics studies
#
</MGRunCard>
<slha>
#*********************************************************************
#                        MadGraph/MadEvent                            *
#*********************************************************************
#   Les Houches friendly file for the SM parameters of MadGraph       *
#         Spectrum and decay widths produced by SMCalc                *
#*********************************************************************
#*Please note the following IMPORTANT issues:                         *
#                                                                     *
#0. REFRAIN from editing this file by hand! Some of the parame-       *
#   ters are not independent                                          *
#   (such as G_Fermi, alpha_em, sin(theta_W),MZ,MW) and serious       *
#   problems might be encountered (such as violation of unitarity     *
#   or gauge invariance).  Always use a calculator.                   *
#                                                                     *
#1. alpha_S(MZ) has been used in the calculation of the parameters*
#   but, for consistency, it will be reset by madgraph to the         *
#   value expected IF the pdfs for collisions with hadrons are        *
#   used. This value is KEPT by madgraph when no pdf are used         *
#   lpp(i)=0 .                                                        *
#                                                                     *
#2. Values of the charm and bottom kinematic (pole) masses are        *
#   those used in the matrix elements and phase space UNLESS they     *
#   are set to ZERO from the start in the model (particles.dat)       *
#   This happens, for example,  when using 5-flavor QCD where         *
#   charm and bottom are treated as partons in the initial state      *
#   and a zero mass might be hardwired in the model definition.       *
#                                                                     *
#*********************************************************************
Block SMINPUTS       # Standard Model inputs
     1          1.37000000E+02   # alpha_em(0)
     2          1.12677045E-05   # G_Fermi
     3          1.18000000E-01   # alpha_s(MZ) SM MSbar
     4          9.11876000E+01   # Z mass (as input parameter)
Block YUKAWA      # Yukawa masses m/v=y/sqrt(2)
#    PDG            YMASS
     5          4.20000000E+00   # mbottom for the Yukawa  y_b
     6          1.64500000E+02   # mtop    for the Yukawa  y_t
    15          1.77700000E+00   # mtau    for the Yukawa  y_ta
Block MASS       #  Mass spectrum (kinematic masses)
#       PDG          Mass
         5      4.70000000E+00   # bottom    pole mass
         6      1.72500000E+02   # top       pole mass
        15      1.77700000E+00   # tau       mass
        23      9.11876000E+01   # Z         mass
        24      8.03989750E+01   # W         mass
        25      1.25000000E+02   # H         mass
#             PDG        Width
DECAY         6      1.40582291E+00   # top width
DECAY        23      2.35745147E+00   # Z   width
DECAY        24      1.97656982E+00   # W   width
```

```
DECAY         25      6.13861611E-03    # H    width
#          BR             NDA          ID1          ID2
       7.80406936E-02     2             4           -4    # BR( H -> c    cbar    )
       6.77447395E-01     2             5           -5    # BR( H -> b    bbar    )
       0.00000000E+00     2             6           -6    # BR( H -> t    tbar    )
       4.07190988E-02     2            15          -15    # BR( H -> tau-  tau+)
       1.28539712E-02     2            23           23    # BR( H -> Z    Z^(*))
       1.18071238E-01     2            24          -24    # BR( H -> W    W^(*))
       3.07160159E-02     2            21           21    # BR( H -> g    g     )
       1.43248873E-03     2            22           22    # BR( H -> A    A     )
</slha>
## END BANNER##
<MGGenerationInfo>
#  Number of Events        :  2000000
#  Integrated weight (pb)  :  2.99330E-01
#  Truncated wgt (pb)      :  0.72344E-04
#  Unit wgt                :  1.49665E-07
</MGGenerationInfo>
</header>
<init>
  2212  2212  0.40000000000E+04  0.40000000000E+04  0  0  10042  10042  3  1
  2.99333E-01  6.76911E-05  0.14976500000E-05  0
</init>
```

Listing A.1: MadGraph card for the LO production sample

The MadGraph card shown is from a LO production sample and hence is missing the appropriate lines describing the hard process of a photon emission from the top decay products.

A.1.2 Parton shower generators for the single lepton MC study

As mentioned in Section 3.3.4, each of the presented parton shower generators have their own implementation of a truth-record.

generator	status code	description
PYTHIA6	1 & 3	stable & hard process
FORTRAN HERWIG	1 & 121-129	stable & hard process
HERWIG++	1 & 11	stable & intermediate particle (except hadrons and incoming beam particles)

Table A.1: Reconstruction efficiencies of the algorithms for different jet configurations.

Table A.1 shows the implementation of the truth record for different MC generators. While the stable particles record is similar for all generators, the hard process particles are more difficult to find for certain generators. The hard process particles are important to differentiate between single lepton and dileptonic $t\bar{t}$ events, as well as for estimating whether an event is truth matched or not. Note that Table A.1 shows only how to find the stable and hard process particles for each generator and does not cover the full particle record.

A.2 Additional figures

A.2.1 MC section

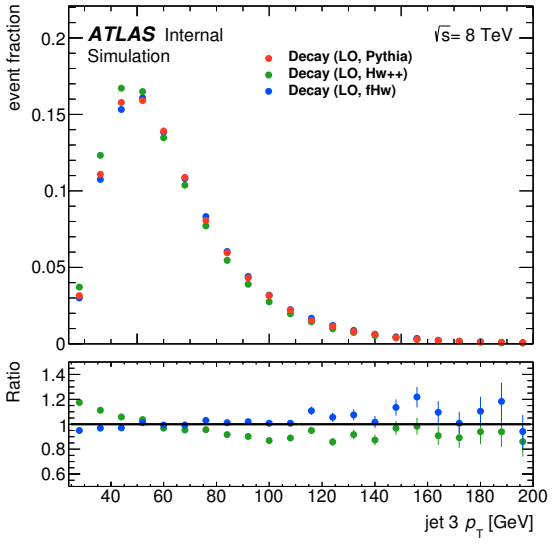

(a) p_T-distribution of the third hardest jet.

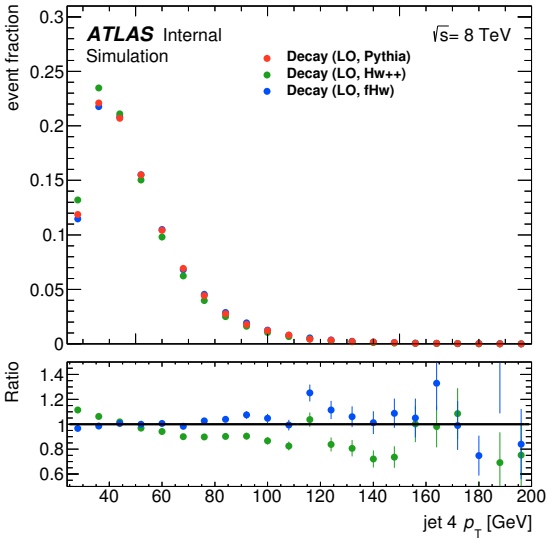

(b) p_T-distribution of the fourth hardest jet.

Figure A.1: p_T distributions of the jets for different parton shower generators.

Figure A.1 shows the p_T distributions of the third and fourth hardest jets in each event, for different parton shower generators. The differences in the shapes are very similar to the distributions of the hardest and second hardest jet and were explained in section 3.3.4.

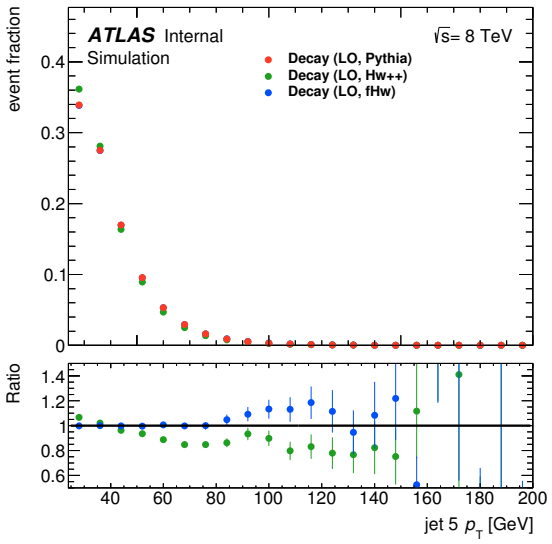

Figure A.2: p_T-distribution of the fifth hardest jet.

Figure A.2 shows the p_T distributions of the fifth hardest jets in each event, as long as the event has 5 jets or more, passing the object selection for jets.

Bibliography

[1] K. A. Olive et al., *Review of Particle Physics*, Chin. Phys. **C38** (2014) 090001.

[2] ATLAS, CDF, CMS and D0 Collaborations,
First combination of Tevatron and LHC measurements of the top-quark mass (2014),
arXiv: 1403.4427 [hep-ex].

[3] P. W. Higgs, *Broken Symmetries and the Masses of Gauge Bosons*,
Phys. Rev. Lett. **13** () 508–509,
URL: http://link.aps.org/doi/10.1103/PhysRevLett.13.508.

[4] F. Englert and R. Brout, *Broken Symmetry and the Mass of Gauge Vector Mesons*,
Phys. Rev. Lett. **13** (1964) 321–323.

[5] ATLAS Collaboration, *Observation of a new particle in the search for the Standard Model Higgs boson with the ATLAS detector at the LHC*, Phys. Lett. **B716** (2012) 1–29,
arXiv: 1207.7214 [hep-ex].

[6] S. Chatrchyan et al.,
Observation of a new boson at a mass of 125 GeV with the CMS experiment at the LHC,
Phys. Lett. **B716** (2012) 30–61, arXiv: 1207.7235 [hep-ex].

[7] Y. Fukuda et al., *Evidence for oscillation of atmospheric neutrinos*,
Phys. Rev. Lett. **81** (1998) 1562–1567, arXiv: hep-ex/9807003 [hep-ex].

[8] F. P. An et al., *New Measurement of Antineutrino Oscillation with the Full Detector Configuration at Daya Bay*, Phys. Rev. Lett. **115** (2015) 111802,
arXiv: 1505.03456 [hep-ex].

[9] F. Abe et al.,
Observation of Top Quark Production in $p\bar{p}$ Collisions with the Collider Detector at Fermilab,
Phys. Rev. Lett. **74** (1995) 2626–2631,
URL: http://link.aps.org/doi/10.1103/PhysRevLett.74.2626.

[10] S. Abachi et al., *Observation of the top quark*, Phys. Rev. Lett. **74** (1995) 2632–2637,
arXiv: hep-ex/9503003 [hep-ex].

[11] ATLAS Collaboration, *Improved luminosity determination in pp collisions at $\sqrt{s} = 7$ TeV using the ATLAS detector at the LHC*, Eur. Phys. J. **C73** (2013) 2518, arXiv: 1302.4393 [hep-ex].

[12] ATLAS Collaboration, *The ATLAS Experiment at the CERN Large Hadron Collider*,
JINST **3** (2008) S08003.

[13] S. Chatrchyan et al., *The CMS experiment at the CERN LHC*, JINST **3** (2008) S08004.

[14] K. Aamodt et al., *The ALICE experiment at the CERN LHC*, JINST **3** (2008) S08002.

[15] A. A. Alves Jr. et al., *The LHCb Detector at the LHC*, JINST **3** (2008) S08005.

[16] M. H. Seymour and M. Marx, *Monte Carlo Event Generators* (2013) 287–319, arXiv: 1304.6677 [hep-ph].

[17] R. Placakyte, *Parton Distribution Functions* (2011), arXiv: 1111.5452 [hep-ph].

[18] S. Alioli et al., *A general framework for implementing NLO calculations in shower Monte Carlo programs: the POWHEG BOX*, JHEP **06** (2010) 043, arXiv: 1002.2581 [hep-ph].

[19] T. Sjostrand, S. Mrenna and P. Z. Skands, *PYTHIA 6.4 Physics and Manual*, JHEP (2006) 026, arXiv: hep-ph/0603175 [hep-ph].

[20] J. A. Aguilar-Saavedra et al., *Shedding light on the $t\bar{t}$ asymmetry: the photon handle*, JHEP **04** (2014) 188, arXiv: 1402.3598 [hep-ph].

[21] K. Melnikov, M. Schulze and A. Scharf, *QCD corrections to top quark pair production in association with a photon at hadron colliders*, Phys. Rev. **D83** (2011) 074013, arXiv: 1102.1967 [hep-ph].

[22] ATLAS Collaboration, *Observation of top-quark pair production in association with a photon and measurement of the $t\bar{t}\gamma$ production cross section in pp collisions at $\sqrt{s} = 7$ TeV using the ATLAS detector*, Phys. Rev. **D91** (2015) 072007, arXiv: 1502.00586 [hep-ex].

[23] CMS Collaboration, *Measurement of the inclusive top-quark pair + photon production cross section in the muon + jets channel in pp collisions at 8 TeV*, **CMS-PAS-TOP-13-011** ().

[24] P. Golonka and Z. Was, *PHOTOS Monte Carlo: A Precision tool for QED corrections in Z and W decays*, Eur. Phys. J. **C45** (2006) 97–107, arXiv: hep-ph/0506026 [hep-ph].

[25] J. Alwall et al., *MadGraph 5 : Going Beyond*, JHEP **06** (2011) 128, arXiv: 1106.0522 [hep-ph].

[26] A. Kardos and Z. Trócsányi, *Hadroproduction of t anti-t pair in association with an isolated photon at NLO accuracy matched with parton shower*, JHEP **05** (2015) 090, arXiv: 1406.2324 [hep-ph].

[27] G. Bevilacqua et al., *HELAC-NLO*, Comput. Phys. Commun. **184** (2013) 986–997, arXiv: 1110.1499 [hep-ph].

[28] ATLAS Collaboration, *Comparison of Monte Carlo generator predictions for gap fraction and jet multiplicity observables in top-antitop events*, ATL-PHYS-PUB-2014-005 (), URL: http://cds.cern.ch/record/1703034.

[29] G. Corcella et al., *HERWIG 6: An Event generator for hadron emission reactions with interfering gluons (including supersymmetric processes)*, JHEP **01** (2001) 010, arXiv: hep-ph/0011363 [hep-ph].

[30] S. Gieseke, "The New Monte Carlo event generator Herwig++", *Deep inelastic scattering. Proceedings, 12th International Workshop, DIS 2004, Strbske Pleso, Slovakia, April 14-18, 2004. Vol. 1 + 2*, 2004 602–605, arXiv: hep-ph/0408034 [hep-ph], URL: http://www.saske.sk/dis04/proceedings/C/gieseke.ps.gz.

[31] ATLAS Collaboration, *New ATLAS event generator tunes to 2010 data*, ATL-PHYS-PUB-2011-008 (), URL: http://cds.cern.ch/record/1345343.

[32] M. Bahr et al., *Herwig++ Physics and Manual*, Eur. Phys. J. **C58** (2008) 639–707, arXiv: 0803.0883 [hep-ph].

[33] K. Hamilton and P. Richardson,
Simulation of QED radiation in particle decays using the YFS formalism, JHEP **07** (2006) 010, arXiv: hep-ph/0603034 [hep-ph].

[34] U. Baur et al., *Probing electroweak top quark couplings at hadron colliders*,
Phys. Rev. **D71** (2005) 054013, arXiv: hep-ph/0412021 [hep-ph].

[35] ATLAS Collaboration, *Measurement of the b-tag Efficiency in a Sample of Jets Containing Muons with 5 fb-1 of Data from the ATLAS Detector*, ATLAS-CONF-2012-043 (), URL: http://cds.cern.ch/record/1435197.

[36] ATLAS Collaboration,
Measurement of the Mistag Rate with 5 fb^{-1} of Data Collected by the ATLAS Detector, ATLAS-CONF-2012-040 (), URL: http://cds.cern.ch/record/1435194.

[37] J. Erdmann et al.,
A likelihood-based reconstruction algorithm for top-quark pairs and the KLFitter framework, Nucl.Instrum.Meth. **A748** (2014) 18–25, arXiv: 1312.5595 [hep-ex].

[38] ATLAS Collaboration, *Measurement of the $t\bar{t}$ production cross-section using $e\mu$ events with b -tagged jets in pp collisions at $\sqrt{s}$ = 7 and 8 TeV with the ATLAS detector*,
Eur. Phys. J. **C74** (2014) 3109, arXiv: 1406.5375 [hep-ex].

[39] W. Lukas, *Fast Simulation for ATLAS: Atlfast-II and ISF* (2012), URL:
http://cdsweb.cern.ch/record/1458503/files/ATL-SOFT-PROC-2012-065.pdf.

[40] M. Cacciari and G. P. Salam, *Dispelling the N^3 myth for the k_t jet-finder*,
Phys. Lett. **B641** (2006) 57–61, arXiv: hep-ph/0512210 [hep-ph].

[41] ATLAS Collaboration, *Performance of b-Jet Identification in the ATLAS Experiment* (2015), arXiv: 1512.01094 [hep-ex].

[42] ATLAS Collaboration, *Measurements of the photon identification efficiency with the ATLAS detector using* 4.9 fb^{-1} *of pp collision data collected in 2011*, ATLAS-CONF-2012-123, URL: http://cdsweb.cern.ch/record/1473426.

[43] ATLAS Collaboration, *Improved luminosity determination in pp collisions at sqrt(s) = 7 TeV using the ATLAS detector at the LHC*, Eur. Phys. J. **C73** (2013) 2518,
arXiv: 1302.4393 [hep-ex].

List of Figures

List of Tables